Discovery of Selective Nanomolar Inhibitors for Insulin-Regulated Aminopeptidase Based on α-Hydroxy-β-Amino Acid Derivatives of Bestatin

Dionisios Vourloumis,[1,†,‡] Ioannis Mavridis,[1,‡] Alexandros Athanasoulis,[1] Ioannis Temponeras,[1] Despoina Koumantou,[1] Petros Giastas,[2] Anastasia Mpakali,[1,3] Victoria Magrioti,[3] Jacqueline Leib,[4] Peter van Endert,[4,5] Efstratios Stratikos,[1,3,*] and Athanasios Papakyriakou[1,*]

[1] National Centre for Scientific Research "Demokritos", GR-15341 Ag. Paraskevi, Athens, Greece

[2] Department of Biotechnology, Agricultural University of Athens, GR-11855 Athens, Greece

[3] Department of Chemistry, National and Kapodistrian University of Athens, GR-15784, Athens, Greece

[4] Université Paris Cité, INSERM, CNRS, Institut Necker Enfants Malades, F-75015 Paris, France

[5] Service Immunologie Biologique, AP-HP, Hôpital Universitaire Necker-Enfants Malades, F-75015, Paris, France

[†] *In memory of our beloved colleague who passed away on 21st March 2020*

[‡] These authors contributed equally

[*] Corresponding authors: estratikos@chem.uoa.gr | thpap@bio.demokritos.gr

Abstract. The oxytocinase subfamily of M1 zinc aminopeptidases comprises emerging drug targets, including the ER-resident aminopeptidases 1 and 2 (ERAP1 and ERAP2), and insulin-regulated aminopeptidase (IRAP), however, reports on clinically relevant inhibitors are limited. Here we report a new synthetic approach of high diastereo- and regio-selectivity for functionalization of the α-hydroxy-β-amino acid scaffold of bestatin. Stereochemistry and mechanism of inhibition were investigated by a high-resolution X-ray crystal structure of ERAP1 in complex with a micromolar inhibitor. By exploring the P1 side-chain functionalities, we achieve significant potency and selectivity, and we report a cell-active, low nanomolar inhibitor of IRAP with >120-fold selectivity over homologous enzymes. X-ray crystallographic analysis of IRAP in complex with this inhibitor suggest that interactions with the GAMEN loop is an unappreciated key determinant for potency and selectivity. Overall, our results suggest that α-hydroxy-β-amino acid derivatives may constitute useful chemical tools and drug leads for this group of aminopeptidases.

Keywords: Functionalized oxazolidine, common intermediate, α-hydroxy-β-amino acid, zinc chelate, IRAP, ERAP1, ERAP2, M1 zinc aminopeptidase, design, synthesis, biochemical evaluation, X-ray crystal structure

INTRODUCTION

M1 aminopeptidases constitute one of the major family of aminopeptidases, enzymes that catalyze the removal of amino acids from the N-terminus of polypeptides. All members of this family are zinc-dependent enzymes that carry two conserved sequence motifs that are critical to their catalytic function: the HEXXH-(X_{18})-E motif that is necessary to zinc binding and the GXMEN exopeptidase motif that is critical to active site formation and selectivity.[1] M1 aminopeptidases carry out a vast variety of biological functions, several of which are involved in human disease and as a result they are frequent drug targets.[2] In particular, the oxytocinase subfamily of M1 aminopeptidases that consists of ER aminopeptidase 1 and 2 (ERAP1, ERAP2) and Insulin Regulated Aminopeptidase (IRAP) have been the target of active research in drug development.[3-9] These three enzymes play important roles in the function of the immune system, tumorigenesis, blood pressure, intracellular trafficking and cognitive function, thus their pharmacological regulation has been suggested to have important therapeutic applications.[10-12] Consequently, much research has been focused on the role of ERAP1 and ERAP2 in regulating antigen processing and presentation, and on its potential in cancer immunotherapy and control of inflammatory autoimmunity.[13,14] Although IRAP plays important roles in antigen cross-presentation[15] and T-cell receptor signaling,[16] most drug-development efforts to date have focused on its role in cognition.[8] Still, possible applications of IRAP inhibition in cancer immunotherapy or autoimmunity have been emerging,[17] in particular due to its unique role in cross-presentation by dendritic cells,[15,18] an important component of anti-cancer immune responses.[19] Several chemical scaffolds have been explored as IRAP inhibitors (recently reviewed in [11,20,21]). The first IRAP inhibitors were based on the physiological hexapeptide inhibitor of IRAP angiotensin IV,[22] and included linear and macrocyclic analogues.[23,24] The first generation of drug-like, small molecular weight inhibitors of IRAP were discovered through *in silico* screening using a homology model of IRAP and included the pyridine derivative HFI-419 and the quinoline derivatives HFI-435 and HFI-437.[25,26] In addition, two aryl sulfonamides and a spiro-oxindole dihydroquinazolinone were identified after screening a substance library of 10,500 low-molecular-weight compounds.[27-30] Rationally, structure-based designed inhibitors have also been explored, including diaminobenzoic acids and pseudophosphinic peptides.[6,31,32] However, despite several years of small-molecule inhibitors development for these enzymes a clinical application has yet to be reported, suggesting that more drug-like scaffolds need to be explored.

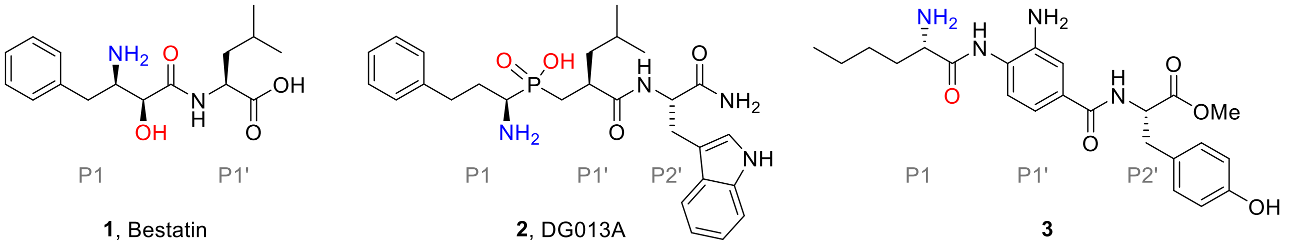

1, Bestatin **2**, DG013A **3**

Chart 1. Structures of bestatin (**1**), the potent phosphinic inhibitor of ERAP1 and IRAP, DG013A (**2**), and a diaminobenzoic acid-based inhibitor of ERAP2 (**3**). Zinc-coordinating atoms are colored red and the α-amine that mimics the substrate's N-terminus is colored blue. Side chains that target the S1, S1′ and S2′ pockets of the enzymes are designated as P1, P1′ and P2′, respectively.

Bestatin is a natural product inhibitor of zinc-aminopeptidases, which was isolated from a culture filtrate of *S. olivoreticuli* by Umezawa.[33,34] The structure of bestatin (Chart 1) is similar to a L-Phe-L-Leu dipeptide, where Phe is an α-hydroxyl-β-amino acid with the absolute stereochemistry of (*2S*,*3R*). Bestatin has been shown to be a modest to weak inhibitor of several families of metallo-aminopeptidases including members of the M1 family.[35-37] It blocks the active site of aminopeptidases in a reversible manner,[38] mainly via chelation to the catalytic zinc and through interaction of the α-amine with one or two acidic residues that flank the entrance of the S1 subsite of the enzyme. Motivated by the clinical application of bestatin that has been marked in Japan as a complementary chemotherapeutic agent in the treatment of acute myeloid leukemia,[39,40] some studies have produced analogues based on its α-hydroxy-β-amino scaffold as inhibitors of metallo-aminopeptidases.[2,41,42] A notable example is the optimization of the bestatin scaffold towards nanomolar inhibitors of PfA-M1 aminopeptidase, an essential parasitic enzyme of potential therapeutic value.[42] For the synthesis of these analogues, commercially available D-amino acids were transformed into α-amino aldehydes, followed by Wittig methylenation and dihydroxylation of the resulting alkene. The diastereomeric mixture of the diols was oxidized and the active (*2S*,*3R*) diastereoisomers were purified by reverse phase HPLC. While this synthetic strategy allows preparation of α-hydroxy-L-β-amino acids from α-D-amino acids with good yields, it is limited by the availability of α-D-amino acids for the P1 position and the required separation of diastereoisomers by HPLC. Other routes employed for the preparation of bestatin and derivatives have used chiron approaches starting from amino acids or sugars,[43-45] asymmetric catalysis,[46-50] the Passerini approach,[51] or chemoenzymolysis.[52] However, these methods suffer from poor diastereo- or regio-selectivity, and more importantly, most routes are significantly limited in the diversity of the side chains that can be explored.

Here, we present a synthetic methodology that involves two *N*-Boc protected oxazolidine intermediates with the required stereochemistry to incorporate a series of P1 side-chain moieties, in combination with any P′ substituent coupled at the 5-carboxylate group. The desired stereochemistry is achieved at a high regioselectivity ratio through asymmetric Sharpless aminohydroxylation,[53] which is promoted by protecting groups of appropriate length.[54] The strategic protection of the (*2S*,*3R*)-2-hydroxy-3-amino moiety in an oxazolidine scaffold allowed us to demonstrate the versatility of this approach by introducing a variety of functional groups in the P1 substituent for the generation of potent zinc aminopeptidase inhibitors.[55,56] Many of the synthesized derivatives were found to be sub-micromolar inhibitors of ERAP1, ERAP2 and IRAP. We obtained a high-resolution X-ray crystal structure of ERAP1 in complex with one of these compounds (resolved at 1.6 Å), which verified the required stereochemistry and validated the zinc-binding mode as competitive inhibitor. Three of these compounds displayed low nanomolar inhibition for IRAP (up to IC_{50} of 6.5 nM) with significant selectivity against the highly homologous ERAP1 and ERAP2 (170- and 120-fold for the most selective, respectively). A cross-presentation assay was utilized to confirm their cellular activity for IRAP at sub-micromolar concentrations. The X-ray crystal structure of IRAP in complex with this potent and selective inhibitor revealed structural features of the active site that could be employed in the design of selective inhibitors for the members of the oxytocinase subfamily.

RESULTS AND DISCUSSION

Design and synthesis of the inhibitors

Based on the core scaffold of α-hydroxy-β-amino acid scaffold of bestatin we sought to increase its binding affinity for the three M1 aminopeptidases. This could be achieved by optimizing the P1 side chain that targets the S1 specificity pocket and which is characteristic for each member of the M1 family of aminopeptidases. An early investigation of their S1 specificity profile has revealed that ERAP1 has higher preference for long and hydrophobic aliphatic or aromatic amino acids, ERAP2 displayed high preference for basic amino acids, whereas IRAP was the most permissive and combined the specificity of ERAP1 and ERAP2.[57] In addition to optimization of the P1 substituent, we also opted to target the S2′ subsite of the enzymes for increased potency, while retaining the L-Leu (P1′) of bestatin. Thus, for the primed subsites we used the dipeptides L-Leu-L-Trp, or L-Leu-L-Tyr, both of which have been shown to yield potent inhibitors of aminopeptidases that generate antigenic peptides (**2**, **3** in Chart 1).[5,6]

Although bestatin is used as a general inhibitor of M1 aminopeptidases, its inhibition profile for ERAP1, ERAP2 and IRAP is not documented. So our first goal was the synthesis and biochemical evaluation of bestatin (**1**) and of two key derivatives of bestatin; one with homo-phenylalanine (L-hPhe) instead of phenylalanine as P1 side chain (**8**–**9**, Scheme 1), and another with L-Leu-L-Trp dipeptide instead of a single leucine for the primed sites (**10**–**11**, Scheme 1). The longer side chain of

L-hPhe has been shown to be a good substrate for the S1 subsite of ERAP1 and IRAP,[57] and since then L-hPhe in combination with a dipeptide of natural or non-proteinogenic amino acids targeting the S1′–S2′ subsites has been employed in many high-affinity, nanomolar inhibitors of these aminopeptidases (**2**, **3** in Chart 1).[5,31,58]

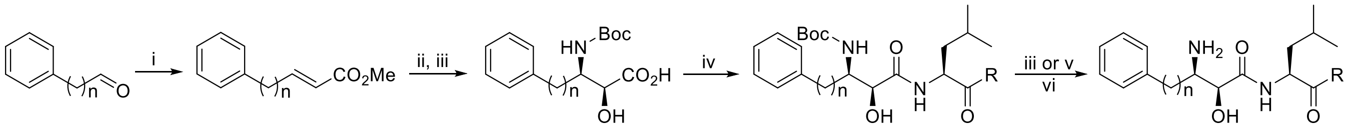

4a n=1
4b n=2

5a n=1
5b n=2

6a n=1
6b n=2

7a, n=1, R=OMe
7b, n=2, R=OMe
7c, n=2, R=L-TrpOBn

1, n=1, R=OH
8, n=2, R=OMe
9, n=2, R=OH
10, n=2, R=L-TrpOBn
11, n=2, R=L-TrpOH

Scheme 1. Synthesis of bestatin (**1**) and initial analogues. i) $Ph_3P{=}CHCOOMe$ (1.2 equiv), CH_2Cl_2, rt, 16 h; ii) NaOH (3 equiv), H_2O, K_2OsO_4 (0.06 equiv), $(DHQD)_2PHAL$ (0.05 equiv), $BocNH_2$ (3 equiv), DCDMH (2 equiv), n-PrOH, rt, 16 h, quenched with Na_2SO_3 (8 equiv); iii) LiOH (2 equiv), H_2O, THF, rt, 1 h; iv) HATU (2.5 equiv), DIPEA (6 equiv), L-Leu-OMe or L-Leu-L-Trp-OBn (1.5 equiv), DMF, 16 h; v) Pd/C (10%), H_2 (1 atm), MeOH, rt, 2 h; vi) TFA:CH_2Cl_2 1:1, rt, 1 h.

The first derivatives were prepared starting from 2-phenylacetaldehyde or 3-phenylpropionaldehyde, which were converted to the corresponding esters **5a** and **5b** through a Wittig reaction (Scheme 1). Introduction of the amino-hydroxyl functionalities at the desired stereochemistry was achieved with Sharpless asymmetric aminohydroxylation, albeit with low regioselectivity as indicated by the low isolated yields of **6a** and **6b** (see Experimental section). The final products were obtained after hydrolysis of the methyl ester (**6a**, **6b**), coupling with L-Leu-OMe or L-Leu-L-Trp-OBn (**7a**–**7c**) and removal of the *N*-Boc protecting group. The carboxy-termini of Leu and Trp were either hydrolyzed to yield the corresponding carboxylic acids (**1**, **9**, **11**), or retained as methyl and benzyl esters, respectively (**8**, **10**).

The next goal was the design of a core scaffold that could be used to functionalize the P1 substituent, the key moiety of an aminopeptidase inhibitor that probes the S1 specificity pocket of the enzymes. As a core scaffold we synthesized a *N*-Boc protected 2,2-dimethyloxazolidine moiety that comprises the central amino-hydroxyl functionality of the inhibitors (**17** and **24**, Scheme 2). The scaffold is functionalized with 5-methylcarboxylate and 4-hydroxyalkyl groups at the appropriate stereochemistry for binding to the active site of M1 aminopeptidases. The hydroxyl group can be readily functionalized to ethers, aldehydes, amines, amides and carboxylic acids to yield a variety of P1 substituents, whereas the length of the final side chain can be controlled starting from either the hydroxymethyl-(**17**) or the hydroxyethyl-(**24**) substituted scaffold. The P′ substituents can be inserted via coupling of amines (carboxy-protected amino acids or peptides) after hydrolysis of the methyl ester, either before, or after functionalization of the P1 substituent. Within the last steps, treatment of the acetal with TFA will furnish the desired (2*S*,3*R*)-2-hydroxy-3-amino moiety of the final products. Synthesis of the core scaffolds **17** and **24** with the appropriate (4*R*,5*S*) stereochemistry was achieved by Sharpless asymmetric aminohydroxylation of **14** and **21**, respectively, with high regio- and stereoselectivity.[54,55] Compound **14** was prepared in two steps from methyl crotonate (**12**), whereas **17** was prepared from 4-hydroxyanisole (**18**) via etherification to **19** followed by Dess-Martin oxidation and Wittig reaction with the appropriate triphenylphosphorane (Scheme 2). Acetal protection using freshly distilled 2-methoxypropene and pyridinium *p*-toluenesulfonate (PPTS), followed by cleavage of the *p*-methoxy ether with ceric ammonium nitrate (CAN) yielded alcohols **17** and **24** (Scheme 2).

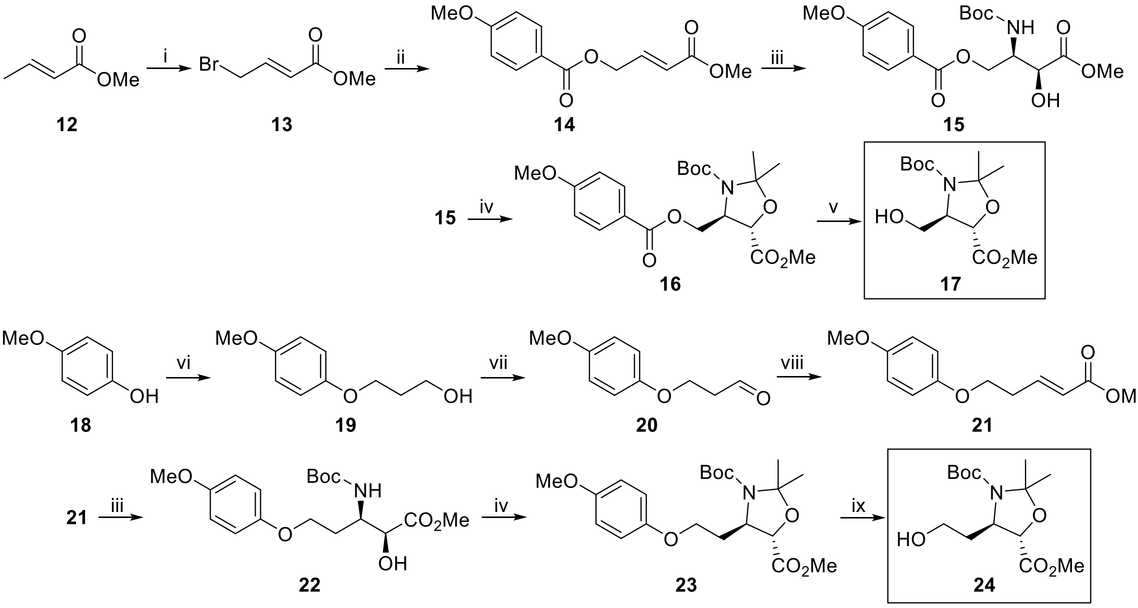

Scheme 2. Synthesis of the key intermediates **17** and **24**. i) NBS (1 equiv), CCl_4, benzyl peroxide (cat), reflux; ii) Cs_2CO_3 (1.2 equiv) *p*-methoxy benzoic acid (1.2 equiv), DMF, rt, 1 h; iii) NaOH (3 equiv), H_2O, K_2OsO_4 (0.06 equiv), $(DHQD)_2PHAL$ (0.05 equiv), $BocNH_2$ (3 equiv), DCDMH (2 equiv), *n*-PrOH, rt, 16 h, quenched with Na_2SO_3 (8 equiv); iv) 2-methoxy propane (20 equiv), PPTS (0.1 equiv), toluene, 25 °C→110 °C, 4 h; v) Cs_2CO_3 (0.6 equiv), MeOH, rt, 16 h; vi) 1,3-propanodiol (1.5 equiv), DIAD (1.8 equiv), PPh_3 (1.7 equiv), THF, reflux, 25 min; vii) Dess-Martin periodinane (2.5 equiv), $NaHCO_3$ (5 equiv), CH_2Cl_2, rt, 2 h; viii) $Ph_3P{=}CHCOOMe$ (1.2 equiv), toluene rt, 16 h; ix) CAN (2 equiv), CH_3CN/H_2O at 0 °C, 30 min.

To demonstrate the flexibility of these core scaffolds as intermediates of potent M1 aminopeptidase inhibitors with a wealth of P1 functionalities and to provide a basis for their preparation, we synthesized and tested a series of compounds as potential inhibitors of three M1 aminopeptidases. As such, **17** and **24** that bear a hydroxymethyl or hydroxyethyl group as P1 can be readily coupled with a dipeptide, after ester hydrolysis, to yield compounds **25** and **26** upon treatment with TFA (Scheme

3). For longer alkyl alcohols, another intermediate can be employed (see below). Upon Mitsunobu etherification of **17** or **24** with commercially available substituted phenols (R-OH in Scheme 3), a series of compounds with aromatic ethers as P1 substituents can be prepared readily. Following typical amide coupling and acidic cleavage (or hydrogenation) of the esters and protecting groups compounds **32a–32m** were obtained in good yields. These compounds were expected to afford promising inhibitors of the three aminopeptidases under study, but also to allow for exploration of the S1 pocket with different substituted aryl groups.

Dess-Martin oxidation of **17** and **24** afforded aldehydes **27a** and **27b**, respectively, which is another set of common intermediates that can be employed for a wealth of P1 functionalizations. Here, we prepared alcohol **30** through a Wittig reaction of **27b** with (2-(benzyloxy)ethyl) bromotriphenylphosphorane to yield **28**, followed by hydrolysis of the methyl ester, Pd-catalyzed hydrogenation to **29**, coupling with a dipeptide and treatment with TFA (Scheme 3). This compound was particularly designed as an extension of the nor-leucine side chain (**3** in Chart 1), which has been successfully employed as P1 substituent in previous works,[6] in order to explore the potential interaction of a P1 hydroxyl. From aldehydes **27a** and **27b** a number of aliphatic carboxylic acids were prepared, starting with a Horner–Wadsworth–Emmons reaction with *tert*-butyl 2-(dimethoxyphosphoryl)acetate to furnish **33a** and **33b**, respectively. Then, following a similar set of steps as described for **32a**–**32m**, carboxylic acids **34a**–**34d** were prepared. Although acidic amino acids do not comprise good substrates for the S1 subsite of ERAP1, ERAP2 or IRAP,[57] other M1 aminopeptidases such as APA display good affinity for P1-acidic side chains.[59]

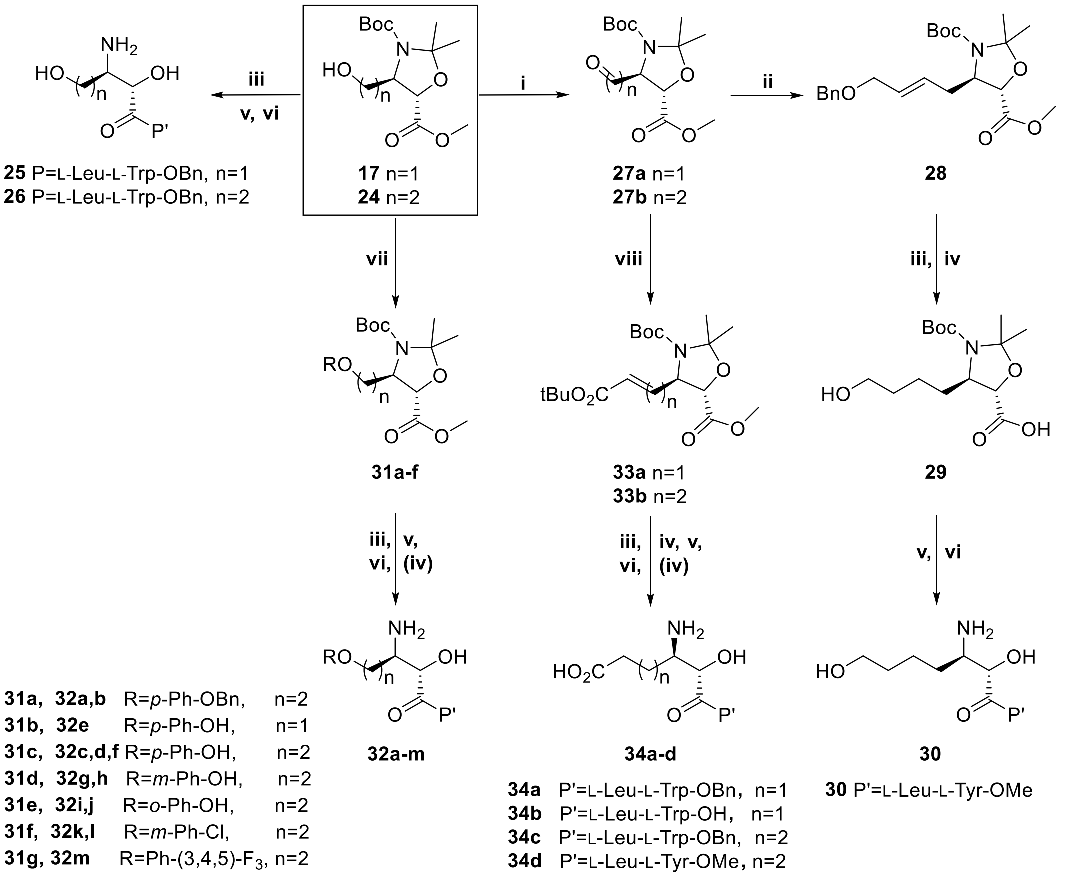
25 P=L-Leu-L-Trp-OBn, n=1
26 P=L-Leu-L-Trp-OBn, n=2
iii
v, vi
17 n=1
24 n=2
i
27a n=1
27b n=2
ii
28
vii
viii
iii, iv
31a-f
33a n=1
33b n=2
29
iii, vi, v, (iv)
iii, vi, iv, v, (iv)
v, vi
31a, 32a,b R=p-Ph-OBn, n=2
31b, 32e R=p-Ph-OH, n=1
31c, 32c,d,f R=p-Ph-OH, n=2
31d, 32g,h R=m-Ph-OH, n=2
31e, 32i,j R=o-Ph-OH, n=2
31f, 32k,l R=m-Ph-Cl, n=2
31g, 32m R=Ph-(3,4,5)-F3, n=2
32a-m
34a-d
34a P'=L-Leu-L-Trp-OBn, n=1
34b P'=L-Leu-L-Trp-OH, n=1
34c P'=L-Leu-L-Trp-OBn, n=2
34d P'=L-Leu-L-Tyr-OMe, n=2
30
30 P'=L-Leu-L-Tyr-OMe

Scheme 3. Synthesis of compounds with aromatic and aliphatic alcohols or carboxylic acids as P1. i) Dess-Martin periodinane (2.5 equiv), $NaHCO_3$ (5 equiv), CH_2Cl_2, rt, 2 h; ii) (2-(benzyloxy)ethyl)bromotriphenyl phosphorane (2.5 equiv), KHMDS (2.5 equiv), toluene, reflux, 2 h; iii) LiOH (2 equiv), H_2O, THF, rt 1–2 h; iv) Pd/C (10%), H_2 (1 atm), MeOH, rt, 3 h; v) dipeptide P′ (1.5 equiv), HATU (2.5 equiv), Et_3N or DIPEA (6 equiv), DMF, rt, 16 h; vi) TFA:CH_2Cl_2 1:1, rt, 1 h; vii) R-OH (1.5 equiv), PPh_3 (1.7 equiv), DIAD (1.8 equiv), THF, 0 °C→reflux, 25 min; viii) *tert*-butyl 2-(dimethoxyphosphoryl)acetate (1.7 equiv), LiHMDS (1.5 equiv), THF, rt, 16 h.

In order to explore other functional groups, **24** was oxidized to the carboxylic acid **35**, which was subsequently coupled with two hydroxyl-alkyl amines for the formation of an amide bond within the P1 substituent (Scheme 4). Through standard coupling and deprotection steps, we obtained **37a** and **37b**, two highly functionalized compounds with a planar amide and one or two hydroxyl groups comprising P1 and L-Leu–L-Trp-OMe as P1′–P2′. A more efficient route for the exploration of different P1 substituents would proceed first by ester hydrolysis and amide coupling of the desired P′ moiety to the common intermediates, and then by functionalization of the P1 alcohol. To demonstrate this route, **38a** and **38b** were prepared from **17** and **24**, respectively (Scheme 4). After Dess-Martin oxidation to the corresponding aldehydes **39a** and **39b**, reductive amination with a series of amines, including amino acids, furnished the amino alkylated analogues **41a–i** after cleavage of the protecting groups. It should be noted however that this route is not always efficient and it is highly dependent on the nature of the P′ substituent with regard to the reaction steps required for functionalization of

P1. For example, we have observed that the hydrogenation reaction required to produce **30** and **34a**–**34d** should precede coupling of the dipeptide (Scheme 3).

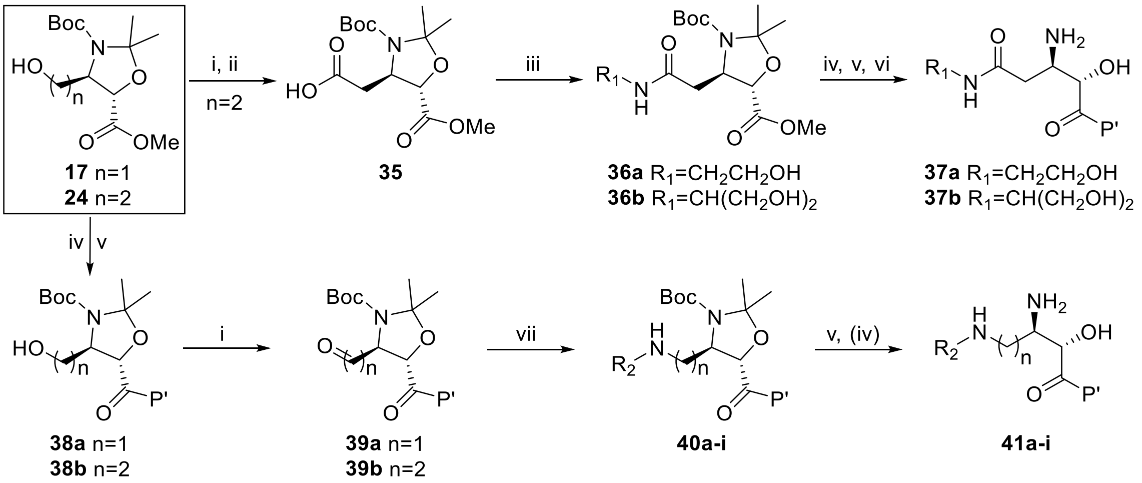

Scheme 4. i) Dess-Martin periodinane (2.5 equiv), $NaHCO_3$ (5 equiv), CH_2Cl_2, rt, 2 h; ii) 2-methylbut-2-ene (10 equiv), $NaClO_2$ (3 equiv), NaH_2PO_4 (3 equiv), *t*-BuOH:THF:H_2O 1:1:1, rt, 45 min; iii) R_1NH_2 (1.2 equiv), HATU (2.5 equiv), Et_3N (6 equiv), DMF 40 °C, 16 h. iv) LiOH (2 equiv), THF:H_2O 3:1, rt, 18 h; v) L-Leu– L-Trp-OMe (1.2 equiv), HATU (2.5 equiv), Et_3N (6 equiv), DMF, rt, 16 h; vi) TFA:CH_2Cl_2 1:1, rt, 1 h; vii) R_2NH_2 shown in Table 2 (3 equiv), $Na(CH_3COO)_3BH$ (3 equiv), dichloroethane, rt, 24 h.

Biochemical evaluation of the inhibitors

To evaluate the capability of the synthesized compounds to act as inhibitors of the oxytocinase subfamily of M1 aminopeptidases, we utilized an established fluorogenic assay using model dipeptide substrates and the recombinant enzymes ERAP1, ERAP2 and IRAP (Tables 1 and 2). Bestatin (**1**) was found to be a poor inhibitor of ERAP1 (IC_{50} = 45 μM) and lacked any observable activity versus ERAP2 or IRAP (IC_{50} >100 μM), consistent with its lack of optimization for the active site of these enzymes. Increasing the side chain length in P1 by substituting Phe with hPhe (**8**, **9**) did not improve the inhibitory effect. However, addition of L-Trp as P2′ in **10** and **11** resulted in a marked improvement of potency for ERAP1 and ERAP2, with considerable, sub-micromolar activity for IRAP, which is consistent with the known pharmacophore requirements of these enzymes.[31,60]

The first two derivatives of intermediates **17** and **24** coupled with L-Leu–L-Trp-OBn (**25** and **26**, respectively) did not display any marked potency, however, a better activity was achieved by increasing the aliphatic chain length of the P1 alcohol in **30** (Table 1). This compound with L-Tyr-OMe as P2′ will be discussed in more detail below as we obtained a high-resolution X-ray crystal structure in complex with recombinant human ERAP1. From the series of the substituted aryl ethers **32a**–**32m** we obtained 7 inhibitors of ERAP1 and 10 inhibitors of ERAP2 with low micromolar activity ($IC_{50} < 2$ μM, Table 1). The highest selectivity for ERAP2 against ERAP1 was displayed by **32g** (18-fold), which however was equipotent for IRAP (IC_{50} of 0.8–1.0 μM). In contrast, we did not obtain any compound with higher selectivity than 4-fold for ERAP1 against ERAP2 (i.e., **30** and **32f**). With regard to IRAP, most of the aryl-ethers in P1 displayed sub-micromolar activity, with 3 compounds displaying low nanomolar activities (IC_{50} values of 6.5–19 nM for **32d**, **32e** and **32m**, Table 1). More importantly, **32e** showed the highest selectivity against ERAP1 (170-fold) and ERAP2 (120-fold). Taken together, we can suggest the *para*-methoxy or *para*-ethoxy phenol, and the 5-ethoxy-1,2,3-trifuorobenzene groups as excellent P1 substituents for obtaining potent inhibitors of the three M1 aminopeptidases employed herein.

Table 1. Biochemical results of compounds **1–32m** against the three homologous M1 aminopeptidases.

ID	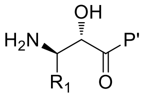		IC_{50} (μM)		
	R_1	**P′**	**ERAP1**	**ERAP2**	**IRAP**
1	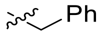	L-Leu-OH	45	>100	>100
8	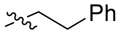	L-Leu-OMe	>100	>100	5.3
9	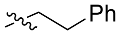	L-Leu-OH	49	>100	>100
10	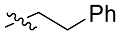	L-Leu– L-Trp-OBn	4.3	1.7	0.28
11	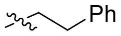	L-Leu– L-Trp-OH	19	17	0.83
25	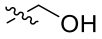	L-Leu– L-Trp-OBn	86	11	5.5
26	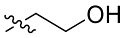	L-Leu– L-Trp-OBn	21	30	2.0
30	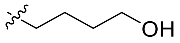	L-Leu– L-Tyr-OMe	1.2	4.9	0.51
32a	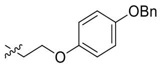	L-Leu– L-Tyr-OMe	30	7.5	0.46
32b	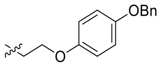	L-Leu– L-Trp-OBn	2.0	5.5	0.24
32c	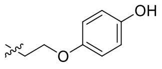	L-Leu– L-Tyr-OMe	1.0	2.3	0.16
32d	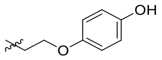	L-Leu– L-Trp-OMe	0.59	0.58	0.013
32e	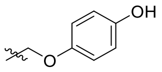	L-Leu– L-Trp-OMe	1.1	0.76	0.0065
32f	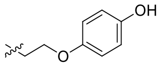	L-Leu– L-Trp-OH	0.48	2.0	0.15
32g	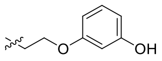	L-Leu– L-Tyr-OMe	18	1.0	0.82
32h	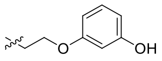	L-Leu– L-Trp-OH	4.6	1.6	0.36

ID	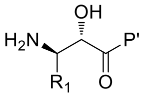		IC_{50} (μM)		
	R$_1$	**P′**	**ERAP1**	**ERAP2**	**IRAP**
32i	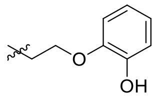	L-Leu–L-Tyr-OMe	22	1.8	4.3
32j	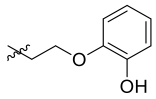	L-Leu–L-Trp-OH	19	1.9	3.1
32k	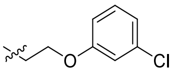	L-Leu–L-Trp-OMe	2.4	0.46	0.20
32l	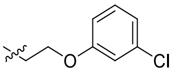	L-Leu–L-Tyr-OMe	8.1	0.58	0.39
32m	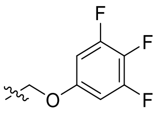	L-Leu–L-Trp-OMe	0.67	0.25	0.019

The remaining compounds that comprise P1 moieties with aliphatic carboxylates (**34a**–**34d**), amides (**37a**–**37b**) and amines (**41a**–**41i**) displayed no inhibition of ERAP1 (up to 100 μM tested) and poor inhibition of ERAP2 and IRAP (Table 2). It should be noted that these compounds were not designed with the aim to obtain potent inhibitors of the targeted aminopeptidases, rather than exhibit the synthetic feasibility and potential to obtain a diverse set of functionalized P1 substituents from the common intermediates **17** and **24** (Schemes 3 and 4). Still, it was interesting to observe that compounds **41e** bearing an ethylaminoethanol moiety, or **41h** carrying a *N*-linked tyrosine amino acid within P1 have the potential to inhibit ERAP2 and IRAP at low micromolar concentrations. The acidic P1 side chains of **34a**–**34d** displayed low affinity for the 3 enzymes, however, similar compounds can be optimal for other M1 aminopeptidases such as aminopeptidase A. Therefore, compounds with acidic moieties targeting the S1 pocket could be a good starting point for development of selective inhibitors for aminopeptidase A, considering their very low affinity for ERAP1, ERAP2 or IRAP.

Table 2. Biochemical results of compounds **34a**–**41i** against the three homologous M1 aminopeptidases.

ID	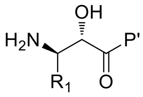		IC_{50} (μM)		
	R$_1$	**P′**	**ERAP1**	**ERAP2**	**IRAP**
34a	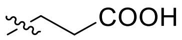	L-Leu–L-Trp-OBn	73	13	43
34b	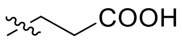	L-Leu–L-Trp-OH	>100	19	>100
34c	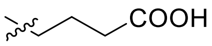	L-Leu–L-Trp-OBn	87	31	31

ID	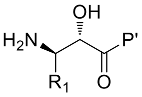		IC$_{50}$ (μM)		
	R$_1$	**P′**	**ERAP1**	**ERAP2**	**IRAP**
34d	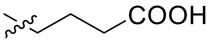	L-Leu– L-Tyr-OMe	>100	13	8.8
37a	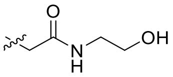	L-Leu– L-Trp-OMe	>100	30	3.9
37b	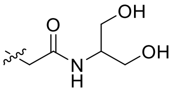	L-Leu– L-Trp-OMe	>100	>100	11
41a	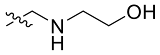	L-Leu– L-Trp-OMe	>100	18	9.0
41b	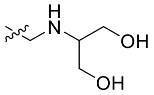	L-Leu– L-Trp-OMe	>100	27	5.0
41c	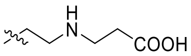	L-Leu– L-Trp-OMe	>100	8.2	7.9
41d	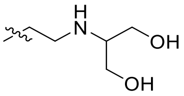	L-Leu– L-Trp-OMe	>100	9.6	8.2
41e	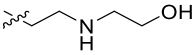	L-Leu– L-Trp-OMe	>100	3.8	1.9
41f	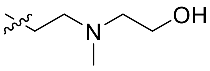	L-Leu– L-Trp-OMe	>100	13	1.5
41g	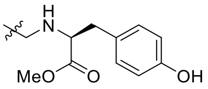	L-Leu– L-Trp-OMe	9.0	1.6	0.27
41h	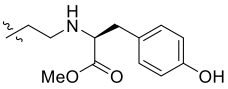	L-Leu– L-Trp-OMe	>100	7.9	0.33
41i	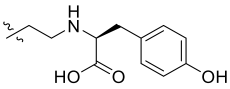	L-Leu– L-Trp-OH	>100	37	13

High-resolution X-ray structure of ERAP1 in complex with inhibitor 30

To better understand the binding configuration and mechanism of inhibition of these derivatives, we used X-ray crystallography to resolve the crystal structure of ERAP1 in complex with compound **30** (Figure 1 A). Crystals that diffracted at 1.6 Å resolution matched the highest resolution reported for this enzyme to date (Table S1).[61] ERAP1 was found in the closed conformation, in which the catalytic site has very limited access to the external solvent and lies adjacent to a large internal cavity (Figure 1 A).[62] Additional electron density was discovered at three locations inside this cavity, in the active site and two allosteric sites previously described.[63] One of those sites in domain IV was interpreted to correspond to binding of a crystallization buffer component, malic acid (MLT).[61] This site has been described before to be able to bind the C-terminus of sufficiently long peptidic substrates, regulate enzymatic activity and is the binding location of a natural product modulator of ERAP1 activity.[63,64] The other allosteric site has been shown before to bind Bis-Tris propane, but here the density was fully attributable to another crystallization buffer component, propylene glycol (PGE, Figure 1 A).[61] This closed conformation of ERAP1 is consistent with inhibitor binding since the open-to-closed conformation transition has been linked with either active site, or allosteric site occupation.[65]

The clear residual electron density within the active site of ERAP1 was used to build an accurate model of **30** (Figure 1 B), which revealed the expected configuration (*2S*,*3R*) for the key 2-hydroxy-3-amino moiety. The 2-hydroxyl carbonyl moiety of **30** acts as a Zn(II) chelating group in the active site, with Zn–L distances of 2.0 Å for L: HO–C and 2.4 Å for L: O=C (Figure S2). The primary amine is stabilized by electrostatic interactions with Glu183, Glu320 and Glu376 in a manner identical to the expected recognition of the N-terminus of a peptidic substrate. The butanol P1 moiety of **30** extends into the elongated S1 pocket of the enzyme, similarly to the P1 side-chain of peptidic substrates,[57] making interactions with the base of the pocket, Met319 all the way to Gln181 (Figure 1 C, D). The depth of the S1 pocket of ERAP1 justifies accommodation of longer P1 groups, such as the *para*-ethoxy-phenol moiety of **32c** and **32d**. We have specifically designed the P1 moiety of **30** to investigate the potential formation of a hydrogen bond with Ser316, however the terminal hydroxyl group formed hydrogen bond with the main-chain C=O of Glu183 (Figure 1 D).

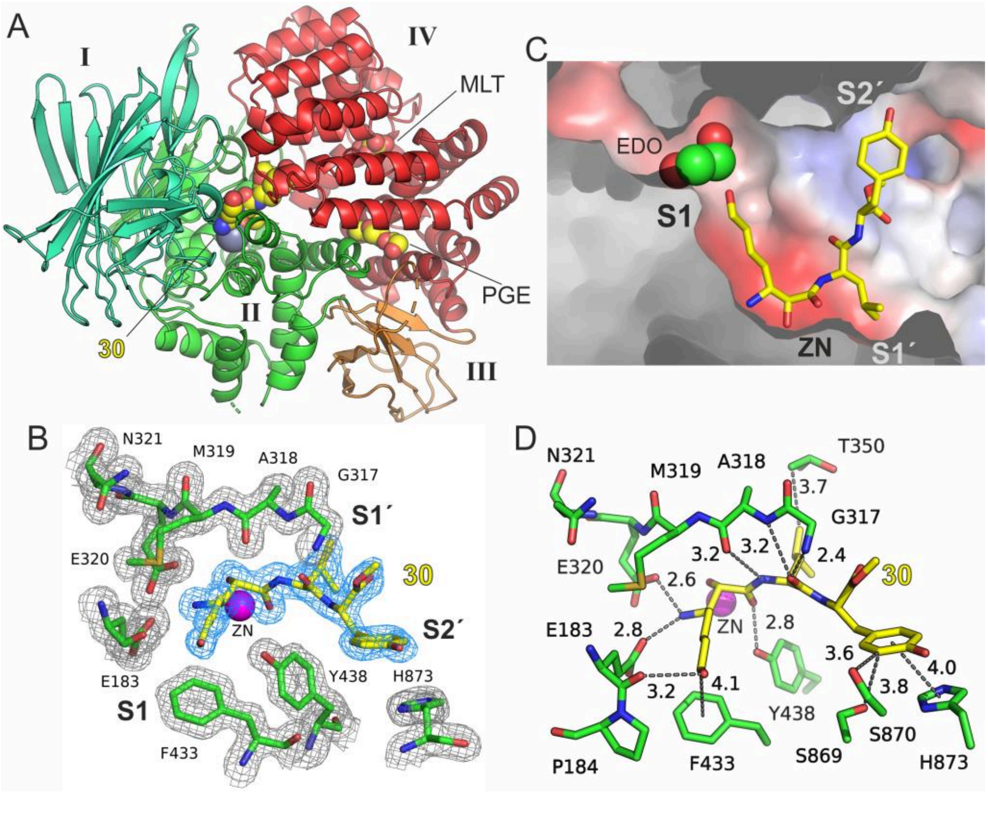
A
I
IV
MLT
II
30
PGE
III
C
S2´
EDO
S1
ZN
S1´
B
N321
M319
A318
G317
S1´
E320
30
ZN
S2´
E183
S1
Y438
H873
F433
D
N321
M319
A318
T350
3.7
G317
E320
3.2
3.2
2.4
30
2.6
E183
2.8
ZN
2.8
3.6
4.0
3.2
4.1
3.8
Y438
S869
S870
H873
P184
F433

Figure 1. **(A)** Cartoon representation of ERAP1 in complex with **30** (PDB ID: 7Z28). Enzyme domains are color-coded as indicated by Latin numbers and the zinc-bound inhibitor is shown with spheres. Two molecules from the crystallization medium were found within domain IV and are indicated (MLT: DL-malic acid, PGE: propylene glycol). **(B)** Close-up view of the active site illustrating the excellent $2F_o–F_c$ electron density map around the inhibitor (density maps are contoured at 1.5σ). ERAP1 residues are colored with green C, blue N and red O atoms, whereas the inhibitor is shown with yellow C atoms. ERAP1 residues comprise of the conserved GAMEN motif, the α-amino docking-site residues Glu183 and Glu320, the catalytic Tyr483 and the aromatic Phe433 and His873 that flank the S1 and S2′ subsites, respectively. **(C)** Surface representation of the active site that is color-coded according to electrostatic potential (red-white-blue from negative to positive), illustrating mainly the geometry and depth of the S1 specificity pocket. An ethylene glycol molecule (EDO) from the crystallization media was found inside the long S1 pocket. **(D)** Close-up view of the active site illustrating the residue-specific interactions of **30**. Distances between heavy atoms or aromatic ring centers are indicated in Å.

The L-Leu moiety of the inhibitor occupies the equivalent of the P1′ side-chain of a substrate and makes a series of van der Waals interactions with a shallow S1′ pocket lined by Thr350, Ala318, His353, Tyr438 and Lys380. The L-Tyr moiety of the inhibitor constitutes an analogue of the P2′ side chain of a substrate and extends away from the active-site Zn(II) towards His873 of domain IV so as to establish a π-stacking interaction (Figure 1 B, D). Overall, the compound binds in the active site of ERAP1 acting as a non-hydrolysable substrate analogue, utilizing the S1, S1′ and S2′ pockets of the enzyme to achieve potency.

Crystal structure of IRAP in complex with the low nanomolar inhibitor 32e

Compound **32e** displayed the highest potency and selectivity for IRAP, being 120–170-fold more potent than ERAP1 and ERAP2 (Table 1). To help understand these properties we obtained a co-crystal structure of IRAP with **32e** that was refined at a final resolution of 2.8 Å (Table S2). IRAP crystallized as a homodimer in the closed state (Figure 2 A), and the residual electron density within the active site could be assigned unambiguously to the zinc-bound inhibitor (Figure S3). Interestingly, the indole group of **32e** within chain B of the dimer could be assigned with two alternative conformations of 0.59/0.41 occupancy (Figure 2 B). Double occupancy was also assigned to the side-chain of Tyr272 in chain A, acting as lid of the S1 pocket (Figure S3). Albeit the lower resolution of the structure with respect to that of ERAP1, the refined model of **32e** was consistent with the expected stereochemistry (*2S*,*3R*) for the 2-hydroxy-3-amino moiety and the bidentate zinc-binding mode. The terminal 3-amino group is docked by the two acidic residues Glu431 and Glu295, and the phenolic group of the P1 substituent is stacked over Phe544 inside the S1 pocket and in a “T-shaped” fashion (Figures 2 B and S3). The main chain atoms of L-Leu form hydrogen bonds with the main chain atoms of Gly428 and Ala429 of the GAMEN-motif, which was found in the closed conformation of IRAP.

As for the P2´ moiety, the indole group was either sandwiched between the phenol group of **32e** and Tyr961 from domain IV (in both chains), or between the catalytic Tyr549 and Tyr961 in the alternative conformation of chain B (Figure S3).

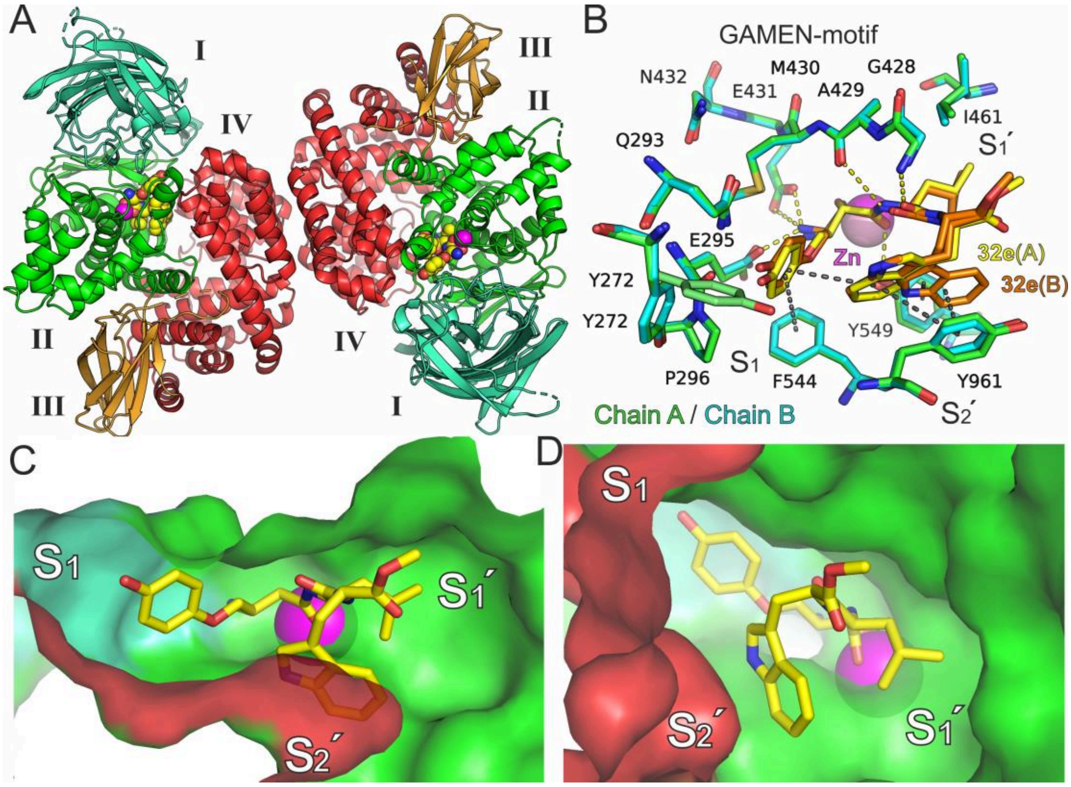

Figure 2. **(A)** Cartoon representation of the IRAP dimer in complex with **32e** (PDB ID: 7ZYF). Domains are color-coded as in Figure 1. **(B)** Superposition of the active sites from chains A (green C atoms) and B (cyan C atoms) illustrating the enzyme–inhibitor interactions. Yellow dashed lines indicate hydrogen bonds and grey dashed lines π–π interactions. Two alternative conformations for **32e** were assigned in chain B (orange C atoms), whereas two alternative conformations for Tyr272 were resolved in chain A. **(C–D)** Surface representation of the substrate binding groove from the top of the active site and from the primed subsites, respectively, illustrating the occupancy of each subsite by the inhibitor. Surfaces are color-coded according to domain as in (A).

The observed binding modes of the inhibitors in the two crystal structures can be used to rationalize the observed structure-activity relationships. Both X-ray structures of ERAP1 and IRAP display an elongated S1 pocket that can accommodate several long, aliphatic and aromatic sidechains (**30–32m**, Table 1). On the other hand, the acid groups of **34a–d** were not well-tolerated in the S1 pocket of ERAP1, likely due to its overall negative electrostatic potential (Figure 1 C). This was also the case for **37a–b** and **41a–41i** that comprise of secondary amines, amides and hydroxyl groups (Table 2), probably due to the narrow shape of the S1 pocket of ERAP1. In contrast, ERAP2 and especially IRAP showed a higher propensity to accommodate branched and polar P1 substituents, a property that may be linked to the functional role of IRAP in the processing of cyclic peptidic substrates (such as oxytocin and vasopressin). This property of IRAP is clearly exemplified in the co-crystal structure with **32e**, where the P2′ indole group of L-Trp is in close proximity (4.6 Å) with the P1 phenolic group in the S1 pocket (Figure 2 C, D).

As clearly demonstrated by the very low affinity of bestatin (**1**) and its analogues **8**–**9** in comparison with derivatives **10** and **11** (Table 1), the presence of a P2′ substituent plays a key role in inhibitor potency for the three enzymes. Now considering the inhibitory effect of similar compounds bearing L-Trp instead of L-Tyr in P2′ (**32b** vs **32a**, **32d** vs **32c, 32k** vs **32l**, Table 1), it is evident that the indole group of Trp provides superior aromatic interactions than the phenolic group of Tyr within the S2′ subsite. Thus, the observed π-stacking interactions of L-Trp with the domain IV residue Tyr961 of IRAP (Figure 2 B) should play a key role in potency.

Regarding the specificity of **32e** for IRAP over ERAP1 and ERAP2, we compared the binding mode of **32e** with those of the pseudophosphinic transition-state analogue DG013A (**2** in Chart 1), which displays equally low nanomolar inhibition for the 3 enzymes (IC_{50} of 48, 80 and 57 nM for ERAP1, ERAP2 and IRAP, respectively).[31] DG013A (**2**) bears the same P1′–P2′ side-chains with 32e, a similar aromatic P1 substituents and has been crystallized in complex with ERAP1 (PDB: 6M8P)[65] and ERAP2 (PDB: 4JBS)[5]. A superposition of the crystal structures of IRAP–**32e** and ERAP1–**2** reveals that **2** could be accommodated within the active site of IRAP in exactly the same conformation as displayed in the X-ray structure of ERAP1 (Figure 3 A, D). However, there's an apparent lack of hydrogen-bonding interactions between **2** and the GAMEN motif residues Gly428–Ala429 that were formed in the X-ray structure of IRAP–**32e**. Now, if **32e** bound to ERAP1 in the same conformation as with IRAP (Figure 3 B), then steric clashes with the GAMEN motif Gly317 and the preceding Ser316 of ERAP1 would most probably impose a conformational change of the L-Trp moiety of **32e** so as to adopt a similar binding mode as **2** in complex with ERAP1 (Figure 3 D). In that conformation however, hydrogen-bonding interactions with the GAMEN motif of IRAP would be compromised. In a similar fashion, if we assume that the L-Leu–L-Trp moiety of **32e** would adopt a similar conformation as **2** upon binding to ERAP2 (Figure 3 C, E), then again it is possible that weak or no hydrogen bonds are formed between the L-Leu main-chain of **32e** and the GAMEN-motif residues Gly334–Ala335 of ERAP2. Taken together, our data suggest that the interactions between the main-chain L-Leu of **32e** and the GAMEN motif of IRAP, in conjunction with appropriate accommodation of the L-Trp side-chain of **32e** within the S2′ pocket are two key determinants for selectivity for IRAP over ERAP1 and ERAP2. As both **32e** and **2** have similar side-chain substituents, it is thus rational to attribute α-hydroxy-β-amino scaffold of **32e** with a greater potential to achieve selectivity for highly homologous aminopeptidases.

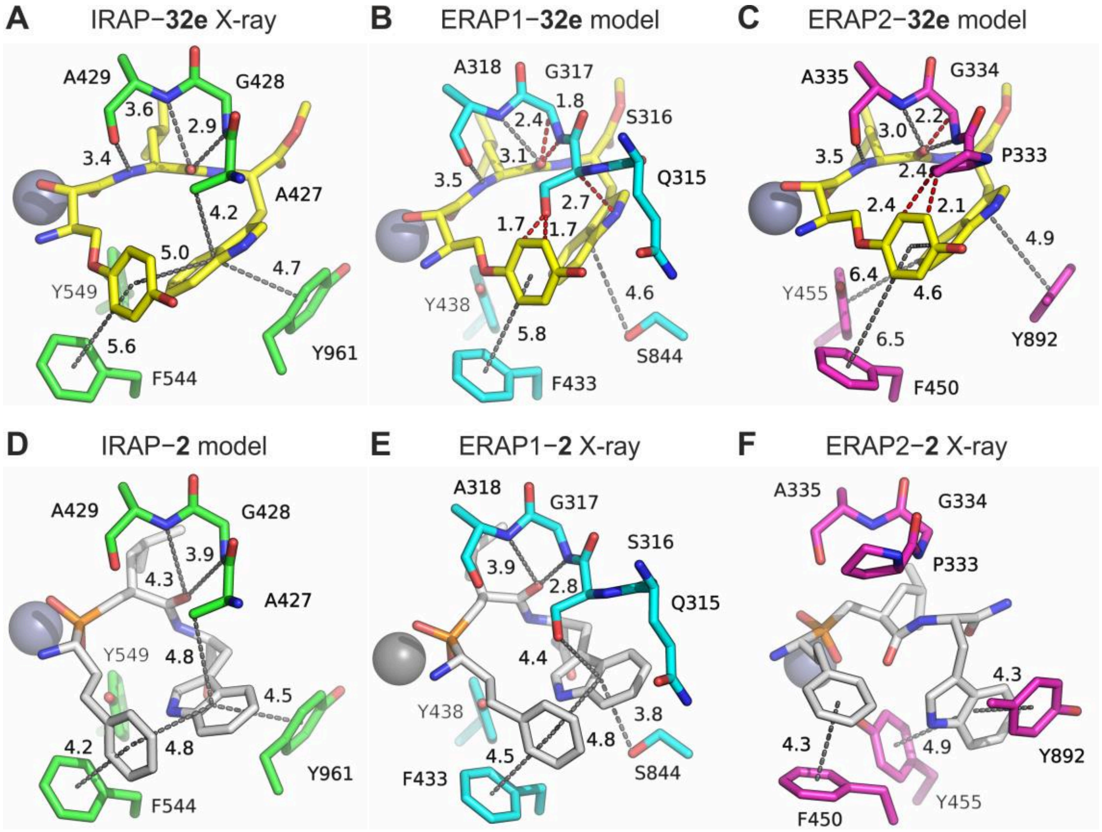
A
IRAP−32e X-ray
A429
G428
3.6
2.9
3.4
A427
4.2
5.0
4.7
Y549
5.6
Y961
F544
B
ERAP1−32e model
A318
G317
1.8
S316
2.4
3.1
Q315
3.5
2.7
1.7
1.7
Y438
4.6
5.8
S844
F433
C
ERAP2−32e model
A335
G334
2.2
3.0
P333
3.5
2.4
2.4
2.1
4.9
Y455
6.4
4.6
6.5
Y892
F450
D
IRAP−2 model
A429
G428
3.9
4.3
A427
Y549
4.8
4.5
4.2
4.8
Y961
F544
E
ERAP1−2 X-ray
A318
G317
S316
3.9
2.8
Q315
4.4
Y438
3.8
4.8
4.5
S844
F433
F
ERAP2−2 X-ray
A335
G334
P333
4.3
4.3
4.9
Y892
F450
Y455

Figure 3. **(A)** Representation of the IRAP active site with bound **32e** (PDB ID: 7ZYF), illustrating potential hydrogen bonds with the GAMEN-motif and aromatic interactions of its indole group. Dashed lines between heavy atoms or aromatic ring centers indicate distances in Å. (**B–C**) Models of **32e** bound to the active sites of ERAP1 **(B)** and ERAP2 **(C)** in the exact same conformation as in **(A)**. Short distances between heavy atoms are indicated by red dashed lines. The models have been obtained by superimposing the X-ray structures of IRAP (this study) with ERAP1 (PDB ID: 6M8P) and ERAP2 (PDB ID: 4JBS). **(D)** Predicted interactions between **2** (DG013A) and the active site residues of IRAP that were obtained from the conformation of **2** bound to ERAP1. **(E–F)** Interactions of **2** within the active site of ERAP1 **(E)** and ERAP2 **(F)** as revealed from crystallographic studies. Views are as similar as possible and comprise of the first two and the preceding residue of the GAMEN loop, the conserved catalytic Tyr(438/455/549), the S1 pocket base Phe(433/450/544), and the key S2′ residue from domain IV Ser844/Tyr892/Tyr961 (ERAP1/ERAP2/IRAP).

Cellular activity of IRAP inhibitors

To investigate the ability of our derivatives to inhibit their target in a cellular context we utilized a recently developed cross-presentation assay (J. Leib and P. van Endert, manuscript in preparation) that relies on the recognition of an ovalbumin epitope presented on the surface of HEK293 cells capable of internalizing immune complexes via Fcγ receptors,[66] and recognized by B3Z hybridoma cells (Figure 4). In this system, cross-presentation of the antigenic epitope is primarily dependent on the enzymatic activity of IRAP as evidenced by the large drop in signal when using IRAP-deficient cells. Titrating increasing amounts of our most potent IRAP inhibitors (**32d** and **32e**, Table 1) resulted in a dose-dependent decrease in T cell activation by WT HEK cells, suggesting that both inhibitors were able to block IRAP activity in this system. Fitting the experimental points to an inhibitor versus response model allowed us to calculate the IC_{50} value for compound **32e** to be 259 nM. Data for compound **32d** followed a very similar trend but had noisier signal that did not allow for a robust fit and an accurate IC_{50} calculation (Figure 4). Some minor effect was observed for the $IRAP^{-/-}$ cells, which may be due to off-target inhibition of ERAP1, which also contributes to cross-presentation.[67] While there is a significant drop-off in potency between the *in vitro* and cell-based assays (7 nM versus 259 nM, a ratio of about 37-fold), compound **32e** was found to still be a potent inhibitor of cross-presentation in a cellular context.

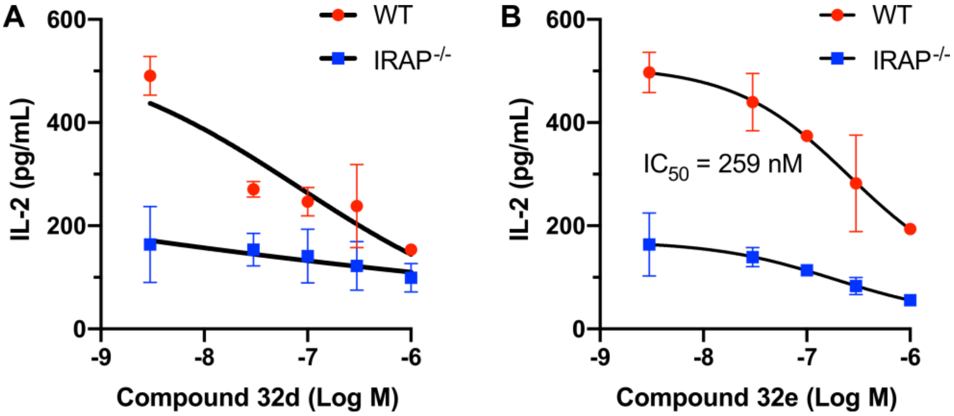

Figure 4. Titration of compounds **32d (A)** and **32e (B)** to HEK293 cells leads to a dose-dependent reduction of cross-presentation of an ovalbumin epitope as followed by IL-2 production by B3Z hybridoma cells. The experiment was also performed using $IRAP^{-/-}$ HEK293 cells to reveal non-IRAP dependent antigen processing. Experimental data points were fit to a variable-slope log(inhibitor) versus response model using GraphPad Prism v8.

Conclusions

Here we utilized a new synthetic approach for the preparation of α-hydroxy-β-amino acid derivatives of bestatin as inhibitors for the oxytocinase sub-family of M1 aminopeptidases. This approach affords the required stereochemistry for binding to the active site zinc, in addition to facile integration of a variety of functional groups that target the S1 specificity pocket of these enzymes. Structure-guided optimization yielded 3 very potent inhibitors of IRAP (IC_{50} of 6.5–19 nM), one of which displayed significant selectivity for the highly homologous ERAP1 and ERAP2 (>120-fold). It should be noted that these inhibitors achieve equal potency to phosphinic pseudopeptides developed before,[31] but without using the transition-state approach that carries higher risk for out-of-family off-target effects and affords a much higher selectivity. Two X-ray crystal structures of a non-selective inhibitor bound to ERAP1, and of the most potent and selective inhibitor bound to IRAP verified the mechanism of inhibition and provided valuable structure-activity information. In particular for IRAP we identified the appropriate aromatic P1 substituent in conjunction with L-Trp for the P2′ substituent and interactions with the GAMEN loop as key factors that contribute to inhibitor potency and selectivity. Our data highlight that main-chain hydrogen bonding with the conserved GAMEN motif should be considered carefully in inhibitor optimization for IRAP. We demonstrate that this class of α-hydroxy-β-amino acids are also potent inhibitors of cross-presentation in a cellular context. Thus, this class of zinc aminopeptidases inhibitors hold promise to be useful tools for cellular and biological investigations, as well as leads for drug discovery efforts.

EXPERIMENTAL SECTION

Materials and methods

Solvents and reagents for organic synthesis were obtained from commercial suppliers and used without further purification, unless otherwise indicated. Reactions requiring anhydrous conditions were carried out in flame-dried (vacuum <0.5 Torr) glassware, using anhydrous, freshly distilled solvents and under an Ar atmosphere. All reactions were stirred with Teflon-coated magnetic stir bars, and temperatures were measured externally. Yields refer to chromatographically and spectroscopically (^{1}H NMR) homogeneous materials. Reactions were monitored by thin-layer chromatography (TLC) carried out on 0.25 mm silica gel plates (60 F254, E. Merck). Silica gel (60, particle size: 0.040–0.063 mm, E. Merck) was used for flash column chromatography. NMR spectra were recorded at 298 K on a Bruker Avance DRX-500, or a Bruker Avance 250 instrument as indicated. The residual undeuterated solvent for ^{1}H NMR [δ_H = 7.26 ($CHCl_3$), 2.50 (DMSO), and 3.31 (MeOH) ppm] and ^{13}C deuterated solvent for ^{13}C NMR [δ_C = 77.16 ($CDCl_3$), 39.52 (DMSO-d_5), and 49.00 (MeOH-d_4) ppm] was used as internal reference. The following abbreviations were used to designate peak multiplicities: s, singlet; d, doublet; t, triplet; q, quartet; m, multiplet; and br, broad. High-resolution mass spectra (HRMS) were measured on a Bruker Maxis Impact QTOF Spectrometer. When required, compounds were further purified by reversed-phase HPLC using a C18 chromolith™ column (Merck, New Jersey, United States) and a 5–50% (*v*/*v*) acetonitrile gradient in water containing 0.05% TFA. Purity of the compounds was validated using a Chromolith® Performance RP-18e 100-4.6 mm column (Merck, New Jersey, United States) using a 13 min 5–50% acetonitrile gradient containing 0.05% TFA at a flow rate of 2 mL/min while following the absorbance at 220 nm. All final compounds employed in the biochemical assays had a purity of at least 95%.

General synthetic procedures

Procedure A: To a stirred solution of the corresponding aldehyde (1.0 mmol) in dichloromethane (5 mL), Wittig ylide Ph_3PCHCO_2Me (401 mg, 1.2 mmol) was added at rt under nitrogen atmosphere. After stirring for 16 h, the solvent was evaporated under reduced pressure and the resulting crude product was purified by column chromatography.

Procedure B: To a stirred solution of *tert*-butyl carbamate (351 mg, 3.0 mmol) in *n*-propanol (2.4 mL) at rt was added a solution of sodium hydroxide (120 mg, 3.0 mmol) in water (7.0 mL). To this mixture was added 1,3-dichloro-5,5-dimethylhydantoin (394 mg, 2 mmol), followed by a solution of $(DHQD)_2PHAL$ (39 mg, 0.05 mmol) in *n*-propanol (2.5 mL), then a solution of the corresponding ester (1.0 mmol) in *n*-propanol (2.5 mL) was added, followed by potassium osmate dihydrate (39 mg, 0.06 mmol).[54] The resulting mixture was stirred at rt overnight, then quenched with sodium sulfite (1.03 g, 8.2 mmol.), diluted with water and extracted into ethyl acetate. The combined organic layers were dried, filtered and concentrated. Purification was done by flash chromatography in Hex/EtOAc to remove the excess of *tert*-butyl carbamate and the second with $MeOH/CH_2Cl_2$ 2→5% for the separation of regioisomers.

Procedure C: The corresponding esters (1.0 mmol) were dissolved in THF and H_2O 3:1 (0.1 M) and then LiOH (2.0 mmol) was added as aqueous solution. The reaction was stirred until completion. The reaction quenched with HCl 1 N and washed with EtOAc. The combined extracts were dried with $MgSO_4$, filtered and concentrated under reduced pressure. Whenever was needed, the crude mixture was purified with flash column chromatography (silica gel, 3→10% MeOH in CH_2Cl_2).

Procedure D: In a dry flask under N_2 the carboxylic acid (1.0 mmol), HATU (2.5 mmol), peptide/amino acid ester (1.5 mmol) are dissolved in dry DMF (1 mL). Et_3N or DIPEA (6 equiv) was added and the reaction mixture was stirred for 16 h at rt. After that, EtOAc was added and the resulting mixture was washed with sat. aqueous solution of $NaHCO_3$ and 1 N aqueous solution of HCl. The aqueous layers were back-extracted with EtOAc (×3) and the combined organic layers were dried over anhydrous Mg_2SO_4, filtered, concentrated and the resulting residues were purified with column chromatography.

Procedure E: A solution of the corresponding ester or alkene (0.057 mmol) in MeOH (2 mL) was treated with 10% Pd/C under an argon atmosphere. The reaction mixture was evacuated and flushed with H_2 gas (four times) and then stirred vigorously under an atmosphere of H_2 (1 atm, H_2) at rt. After 2 h, the reaction mixture was filtered through Celite and concentrated in vacuo to give the crude product which was used for the next synthetic step.

Procedure F: The corresponding intermediate is dissolved in CH_2Cl_2 (1 mL) and TFA (1 mL) is added. The reaction mixture is stirred for 1 h and after that is washed with CH_2Cl_2 and concentrated under reduce pressure until complete removal of residual TFA, resulting in the final, deprotected product.

Procedure G: Alcohol (1.0 equiv) was dissolved in anhydrous THF (0.1 M) along with the corresponding phenol (1.5 equiv) and PPh_3 (1.7 equiv) and the solution was cooled to 0 °C. DIAD (1.8 equiv) was added and the reaction was stirred under reflux for 25 min, cooled to rt and concentrated under reduced pressure. The residue was purified with column chromatography to afford the desired products.

Procedure H: Dess-Martin periodinane (2.5 equiv) and $NaHCO_3$ (5.0 equiv) were added in CH_2Cl_2 (33 mM) and the mixture was stirred for 15 min and cooled to 0 °C before the addition of the corresponding alcohol (1.0 equiv). The reaction was then allowed to warm up to ambient temperature and after stirring for 2 h it was quenched by the addition of a mixture of H_2O / sat. $NaHCO_3$ / sat. $Na_2S_2O_3$ (1:1:1). The occurring biphasic mixture was stirred vigorously for 20 min and extracted with CH_2Cl_2 (×4). The combined organic layers were dried with Mg_2SO_4, filtered and concentrated under reduced pressure.

Procedure I: *tert*-butyl-dimethylphosphonoacetate (1.7 equiv) was dissolved in THF (0.2 M) under Ar and the solution was cooled to 0 °C. LiHMDS (1 M in THF, 1.5 equiv) was then added and the solution was allowed to warm up to ambient temperature. After 0.5 h of stirring the reaction was cooled again to 0 °C, the corresponding aldehyde (1.0 equiv) was added dropwise as a THF solution (0.2 M) and stirring was continued for 16 h at rt. The reaction was then quenched with sat. $NaHCO_3$ washed with brine and washed with EtOAc (×3). The combined organic layers were concentrated under reduced pressure and the residue was purified with column chromatography (10→30% EtOAc/Hex).

Procedure J: Aldehyde (1.0 equiv) was dissolved in *t*-BuOH under Ar atmosphere and an equal volume of 2-methylbut-2-ene 2 M solution in THF (10 equiv) was added. Another equal volume of aqueous solution of $NaClO_2$ (3.0 equiv) and NaH_2PO_4 (3.0 equiv) was added dropwise and the mixture was stirred at rt for 45 min. The reaction was then diluted with CH_2Cl_2, quenched with HCl 1M and washed with CH_2Cl_2 (×3). The combined organic phases were dried over Mg_2SO_4, filtrated, and evaporated under reduced pressure. The resulting residue was purified with column chromatography (5→30% Acetone/Hex).

Procedure K: To a solution of amino alcohol (1.0 equiv) in dry toluene (10 mL) under Ar was added freshly distilled 2-methoxypropene (20 equiv) followed by PPTS (10%). The solution was stirred at rt for 1 h, heated at 110 °C for 3 h and allowed to cool to rt.[54] Saturated sodium hydrogen carbonate solution was added, the organic layer was separated and the aqueous layer was washed with ethyl acetate (3 × 20 mL). The combined organic layers were dried over anhydrous $MgSO_4$, filtered and concentrated under reduced pressure. Purification by flash chromatography gave pure oxazolidine.

Procedure L: The corresponding aldehyde (1.0 equiv) was dissolved under Ar atmosphere in dichloroethane (0.2 M) along with the corresponding amine (3.0 equiv) and $Na(CH_3COO)BH$ (3.0 equiv). The reaction was left to stir at rt for 24 h, quenched with the addition of sat. $NaHCO_3$ and washed with CH_2Cl_2. The combined organic extracts were dried over anhydrous Mg_2SO_4, filtered and concentrated under reduced pressure. The residue was purified with column chromatography using a gradient of 3→10% MeOH/CH_2Cl_2.

***(E)*-methyl 4-phenylbut-2-enoate (5a):** 2-Phenylacetaldehyde (**4a**, 500 mg, 4.16 mmol) was converted to **5a** according to the general procedure A. After column chromatography purification using a gradient of 5%→10% EtOAc/Hex a colorless oil was recovered (R_f=0.5 at 10% EtOAc/Hex, 630 mg, 3.57 mmol). Yield: 85%, ^1H NMR (250 MHz, $CDCl_3$) δ 7.32 (d, J = 14.8 Hz, 2H), 7.29 – 7.08 (m, 4H), 5.84 (d, J = 15 Hz, 1H), 3.73 (s, 3H), 3.53 (d, J = 6.5 Hz, 2H). ^{13}C NMR (63 MHz, $CDCl_3$) δ 166.9, 147.6, 137.6, 128.8, 128.8, 128.7, 128.7, 126.6, 121.9, 51.5, 38.4

***(E)*-methyl 5-phenylpent-2-enoate (5b):** 3-Phenylpropionaldehyde (**4b**, 100 mg, 0.75 mmol) was converted to **5b** according to the general procedure A. After column chromatography purification using a gradient of 10%→20% EtOAc/Hex a colorless oil was recovered (R_f=0.55 at 20% EtOAc/Hex, 122 mg, 0.64 mmol). Yield: 85%. ^1H NMR (500 MHz, $CDCl_3$) δ 7.31 (t, J = 7.4 Hz, 2H), 7.20 (t, J = 7.6 Hz, 3H), 7.03 (dt, J = 15.6, 6.9 Hz, 1H), 5.87 (d, J = 15.7 Hz, 1H), 3.73 (s, 3H), 2.79 (t, J = 7.7 Hz, 2H), 2.54 (q, J = 7.7, 7.3 Hz, 2H). ^{13}C NMR (126 MHz, $CDCl_3$) δ 166.8, 148.2, 140.6, 128.3, 128.3, 128.2, 128.2, 126.0, 121.3, 51.2, 34.2, 33.7

***(2S,3R)*-3-((*tert*-butoxycarbonyl)amino)-2-hydroxy-4-phenylbutanoic acid (6a): 5a** (300 mg, 1.7 mmol) was converted to **6a** (54 mg, 0.176 mmol), a white solid, according to general procedures B and C (52 mg, 0.176 mmol). Isolated yield: 10%; ^1H NMR (500 MHz, CD_3OD) δ 7.47 – 7.17 (m, 5H), 4.27 – 4.01 (m, 2H), 3.00-2.73 (m, 2H), 1.35 (s, 9H). ^{13}C NMR (126 MHz, CD_3OD) δ 176.3, 159.3, 140.5, 131.3, 131.3, 130.3, 130.3, 128.2, 75.9, 74.1, 61.9, 53.45, 25.8, 25.8, 25.8

N-[(2*S*,3*R*)-3-Amino-2-hydroxy-4-phenylbutyryl]-L-leucine (1, bestatin): 6a (50 mg, 0.176 mmol) was converted to **1** (13.5 mg, 0.044 mmol) a white solid following the general procedures D, C and F. Yield: 25%; ^1H NMR (500 MHz, CD_3OD) δ 7.43-7.25 (m, 5H), 4.41 (dd, J = 9.0, 5.2 Hz, 1H), 4.14 (d, J = 3.4 Hz, 1H), 3.75 (q, J = 4.1 Hz, 1H), 3.14 (dd, J = 13.9, 7.8 Hz, 1H), 2.92 (dd, J = 13.9, 7.2 Hz, 1H), 1.81-1.66 (m, 3H), 1.00 (dd, J = 8.2, 5.8 Hz, 6H). ^{13}C NMR (126 MHz, CD_3OD) δ 175.7, 173.6, 136.7, 130.4, 130.1, 128.6, 69.9, 56.45, 52.4, 41.2, 36.4, 26.1, 23.2, 22.0.; ESI HRMS: *m/z* [M + H]+ calcd for $C_{16}H_{25}N_2O_4^+$, 309.1809; found, 309.1809

***(2S,3R)*-3-((*tert*-butoxycarbonyl)amino)-2-hydroxy-5-phenylpentanoic acid (6b): 5b** (100 mg, 0.52 mmol) was converted to **6b** (62 mg, 0.2 mmol), a white solid, according to general procedures B and C. Isolated yield: 38%; ^{1}H NMR (500 MHz, CD$_3$OD) δ 7.31 – 7.10 (m, 5H), 4.19 (d, J = 2.2 Hz, 1H), 4.01 (s, 1H), 2.75 – 2.59 (m, 2H), 1.95 – 1.80 (m, 2H), 1.42 (s, 9H). ^{13}C NMR (126 MHz, CD$_3$OD) δ 176.0, 157.7, 142.9, 129.3, 129.3, 129.2, 129.2, 126.8, 80.1, 73.1, 54.1, 34.9, 33.4, 28.7, 28.7, 28.7

(S)-methyl 2-((2S,3R)-3-amino-2-hydroxy-5-phenylpentanamido)-4-methylpentanoate (8): 6b (43.6 mg, 0.1 mmol) was converted to **8** according to general procedures D and F and a white solid was recovered (19 mg, 0.057 mmol). Yield: 57%; ^{1}H NMR (250 MHz, CD$_3$OD) δ 7.34-7.14 (m, 5H), 4.57-4.42 (m, 1H), 4.31 (d, J = 4.3 Hz, 1H), 3.70 (s, 3H), 3.54-3.37 (m, 1H), 2.87-2.64 (m, 2H), 2.23-2.02 (m, 1H), 1.99-1.79 (m, 1H), 1.76-1.56 (m, 3H), 0.92 (t, J = 7.5 Hz, 6H).^{13}C NMR (63 MHz, CD$_3$OD) δ 174.3, 173.5, 141.7, 129.6, 129.4, 127.4, 70.9, 54.8, 52.81, 52.2, 41.2, 32.4, 32.4, 26.0, 23.2, 21.9. ESI HRMS: *m/z* [M + H]+ calcd for $C_{18}H_{29}N_2O_4^+$, 337.2122; found, 337.2137

***(S)*-2-*((2S,3R)*-3-amino-2-hydroxy-5-phenylpentanamido)-4-methylpentanoic acid (9): 6b** (53 mg, 0.01 mmol) was converted to **9** (24.2 mg, 0.075 mmol) a white solid according to general procedures C and F. Yield: 62%; ^{1}H NMR (250 MHz, CD$_3$OD) δ 7.35-7.11 (m, 5H), 4.54-4.36 (m, 1H), 4.32 (d, J = 4.2 Hz, 1H), 3.48 (td, J = 6.8, 4.1 Hz, 1H), 2.86-2.64 (m, 2H), 2.27-2.02 (m, 1H), 2.02-1.82 (m, 1H), 1.77-1.57 (m, 3H), 0.96 (t, J = 6.6 Hz, 6H). ^{13}C NMR (63 MHz, CD$_3$OD) δ 175.6, 173.5, 141.7, 129.6, 129.3, 127.4, 70.8, 54.8, 52.2, 41.3, 32.4, 32.4, 26.1, 23.3, 21.9.; ESI HRMS: *m/z* [M + H]+ calcd for $C_{17}H_{27}N_2O_4^+$, 323.1966; found, 323.1965

***(6R,7S,10S,13S)*-benzyl 13-((1H-indol-3-yl)methyl)-7-hydroxy-10-isobutyl-2,2-dimethyl-4,8,11-trioxo-6-phenethyl-3-oxa-5,9,12-triazatetradecan-14-oate (7c): 6b** (50 mg, 0.16 mmol) was converted to **7c** according to general procedure D. After column chromatography purification using a gradient of 30%→50% EtOAc/Hex a brown-yellowish oil was recovered (R_f=0.35 at 50% EtOAc/Hex, 64 mg, 0.09 mmol). Yield: 58%. ^{1}H NMR (250 MHz, CDCl$_3$) δ 7.50 (d, J = 7.7 Hz, 1H), 7.44 – 7.02 (m, 13H), 6.89 (s, 1H), 5.35 (d, J = 8.9 Hz, 1H), 5.09 (d, J = 6.8 Hz, 2H), 4.95 (q, J = 6.1 Hz, 1H), 4.70-4.50 (m, 1H), 3.91 (s, 2H), 3.38 – 3.20 (m, 2H), 285-2.49 (m, 2H), 2.00-1.77 (m, 2H), 1.69 – 1.35 (m, 11H), 0.99-0.71 (m, 6H). ^{13}C NMR (63 MHz, CDCl$_3$) δ 173.0, 172.3, 171.6, 156.9, 141.7, 136.2, 135.3, 128.7, 128.7, 128.6, 128.5, 128.5, 128.5, 128.5, 128.4, 128.4, 127.6, 126.0, 123.6, 122.1, 119.5, 118.6, 111.5, 109.3, 80.1, 73.8, 67.4, 53.5, 53.1, 51.2, 40.9, 32.6, 29.8, 28.5, 28.5, 28.5, 27.6, 24.7, 23.0, 21.8

(*S*)-benzyl 2-((*S*)-2-((2*S*,3*R*)-3-amino-2-hydroxy-5-phenylpentanamido)-4-methylpentanamido)-3-(1H-indol-2-yl)propanoate (10): 7c (20 mg, 0.028 mmol) was converted to **10** according to general procedure F. After column chromatography purification using a gradient of 5%→10% MeOH/CH_2Cl_2 a white solid was recovered (10 mg, 0.017 mmol). Yield: 59%. ^{1}H NMR (500 MHz, CD_3OD) δ 7.56-7.47 (m, 1H), 7.37-6.97 (m, 14H), 5.03 (s, 2H), 4.75 (t, J = 6.9 Hz, 1H), 4.45 (dd, J = 8.8, 6.0 Hz, 1H), 4.02 (d, J = 3.6 Hz, 1H), 3.27 (dd, J = 14.6, 7.3 Hz, 1H), 3.21 (dd, J = 14.6, 7.3 Hz, 1H), 3.05 (ddd, J = 7.9, 5.6, 3.6 Hz, 1H), 2.75 (m, 1H), 2.63 (m, 1H), 1.89 (m, 1H), 1.72-1.61 (m, 1H), 1.59-1.45 (m, 3H), 0.85 (dd, J = 12.5, 6.3 Hz, 6H). ^{13}C NMR (63 MHz, CD_3OD) δ 174.3, 173.1, 173.1, 141.6, 138.0, 136.9, 129.6, 129.5, 129.3, 129.3, 128.7, 127.4, 124.7, 122.5, 119.9, 119.2, 112.4, 110.4, 70.7, 68.1, 55.2, 54.7, 53.0, 41.9, 32.4, 32.4 28.4, 25.8, 23.2, 22.1. ESI HRMS: *m/z* [M + H]+ calcd for $C_{35}H_{43}N_4O_5^+$, 599.3228; found, 599.3233

***(S)*-2-(*(S)*-2-(*(2S,3R)*-3-amino-2-hydroxy-5-phenylpentanamido)-4-methylpentanamido)-3-(1H-indol-2-yl)propanoic acid (11): 7c** (40 mg, 0.057 mmol) was converted to **11** according to general procedures E and F. After column chromatography purification using a gradient of 20%→100% MeOH/CH_2Cl_2, 5% AcOH, a white solid was recovered (R_f=0.42 at 20% MeOH/CH_2Cl_2, 14.3 mg, 0.028 mmol). Yield: 50%. ^{1}H NMR (500 MHz, CD_3OD) δ 7.57 (d, J = 7.8 Hz, 1H), 7.33 – 7.13 (m, 6H), 7.09 (s, 1H), 7.04 (t, J = 7.5 Hz, 1H), 6.97 (t, J = 7.4 Hz, 1H), 4.53 (t, J = 5.7 Hz, 1H), 4.30 (dd, J = 10.1, 4.4 Hz, 1H), 4.24 (d, J = 2.9 Hz, 1H), 3.43-3.33 (m, 2H), 3.21 (dd, J = 14.6, 6.6 Hz, 1H), 2.79-2.63 (m, 2H), 2.07-1.95 (m, 1H), 1.87-1.75 (m, 1H), 1.58-1.30 (m, 3H), 0.82 (dd, J = 23.0, 5.8 Hz, 6H).^{13}C NMR (63 MHz, CD_3OD) δ 174.9, 174.2, 173.2, 141.7, 138.0, 129.6, 129.3, 129.3, 128.8, 127.4, 124.6, 122.4, 119.8, 119.3, 112.3, 110.8, 70.7, 54.7, 54.7, 53.2, 41.8, 32.4, 32.42, 28.3, 25.8, 23.2, 22.1.; ESI HRMS: *m/z* [M + H]$^+$ calcd for $C_{28}H_{37}N_4O_5^+$, 509.2758; found, 509.2760

Methyl 4-Bromocrotonate (13). A solution of methyl crotonate (**12**, 1.0 g, 10 mmol) and N-bromosuccinimide (1.78 g, 10 mmol) in CCl_4 (14 mL), containing some crystals of benzoyl peroxide, was heated at reflux for 5 h. After cooling, the reaction mixture was filtered. The filtrate was dried, evaporated and the oily residue was distilled under reduced pressure to give the title compound, bp 80 ^{o}C / 20 mmHg. (R_f=0.4 at 10% EtOAc/Hex, 1.55 g, 8.7 mmol) Yield: 87%.

***(E)*-4-methoxy-4-oxobut-2-en-1-yl 4-methoxybenzoate (14):** Solution of Cs_2CO_3 (2.2 g, 6.7 mmol), 4-MeO-benzoic acid (1.2 g, 6.5 mmol) in 5 mL DMF stirred at rt for 10 min and methyl 4-bromocrotonate (**13,** 1.0 g, 5.6 mmol) was added and stirred at rt for 1 h. Extraction with H_2O and EtOAc (×3), drying with $MgSO_4$, concentration and column chromatography purification, using a gradient of 10%→30% EtOAc/Hex furnished a colorless oil. (R_f=0.3 at 20% EtOAc/Hex, 1.1 g, 4.4 mmol) Yield: 65%. ^{1}H NMR (500 MHz, $CDCl_3$) δ 8.01 (d, J = 8.1 Hz, 2H), 7.05 (d, J = 15.7 Hz, 1H), 6.92 (d, *J* = 8.1 Hz, 2H), 6.11 (d, *J* = 15.6 Hz, 1H), 4.95 (s, 2H), 3.85 (s, 3H), 3.74 (s, 3H). ^{13}C *δ* 166.4, 165.6, 163.8, 142.0, 131.9, 131.8, 121.8, 121.5, 114.3, 113.9, 62.8, 55.7, 51.2

(2R,3S)-2-((*tert*-butoxycarbonyl)amino)-3-hydroxy-4-methoxy-4-oxobutyl 4-methoxybenzoate (15): 14 (1 g, 4 mmol) was converted to **15** according to the general procedure B. After column chromatography purification using a gradient of 30%→60% EtOAc/Hex a white solid was recovered (R_f=0.33 at 50% EtOAc/Hex, 1.3 g, 3.39 mmol). Yield: 85%. ^{1}H NMR (500 MHz, $CDCl_3$) *δ* 7.98 (d, *J* = 8.8 Hz, 2H), 6.89 (d, *J* = 8.9 Hz, 2H), 5.00 (d, *J* = 9.4 Hz, 1H), 4.55-4.45 (m, 1H), 4.43 – 4.30 (m, 3H), 3.84 (s, 3H), 3.79 (s, 3H), 3.03 (s, 1H), 1.38 (s, 9H). ^{13}C NMR (126 MHz, $CDCl_3$) *δ* 173.5, 166.1, 163.7, 155.3, 131.9, 131.9, 122.3, 113.8, 113.8, 80.1, 69.9, 63.4, 55.6, 53.1, 51.9, 28.3, 28.3, 28.3

***(4R,5S)*-3-*tert*-butyl 5-methyl 4-(((4-methoxybenzoyl)oxy)methyl)-2,2-dimethyloxazolidine-3,5-dicarboxylate (16): 15** (600 mg, 1.56 mmol) was converted to **16** according to general procedure K. After column chromatography purification using a gradient of 20%→40% EtOAc/Hex, a colorless oil was recovered (R_f= 0.49 at 40% EtOAc/Hex, 650 mg, 1.53 mmol). Yield: 98%. ^{1}H NMR (500 MHz, $CDCl_3$) *δ* 7.93 (d, *J* = 8.5 Hz, 2H), 6.85 (d, *J* = 8.5 Hz, 2H), 4.66 – 4.31 (m, 4H), 3.78 (s, 3H), 3.72 (s, 3H), 1.59-1.48 (m, 6H), 1.42 (s, 9H). ^{13}C NMR (126 MHz, $CDCl_3$) *δ* 171.3, 165.7, 163.6, 151.1, 131.7, 131.7, 122.2, 113.7, 113.7, 96.5, 80.9, 75.8, 63.17, 58.6, 55.4, 52.5, 28.3, 28.3, 28.3, 27.2 26.2

(4R,5S)-3-*tert*-butyl 5-methyl 4-(hydroxymethyl)-2,2-dimethyloxazolidine-3,5-dicarboxylate (17): Caesium carbonate (127 mg, 0.92 mmol) and p-methoxybenzoyl ester **16** (650 mg, 1.53 mmol) were combined and dissolved in dry methanol (10 mL). The reaction was stirred for 16 h at rt, under an atmosphere of nitrogen. Ammonium chloride solution (sat. 30 mL) was added and the crude product was extracted into ethyl acetate (3 × 100 mL). The combined organic layers were dried (Mg_2SO_4), filtered and concentrated under reduced pressure. Flash chromatographic purification using a gradient of 30%→50% EtOAc/Hex gave pure alcohol **17** as a viscous clear, colorless oil (R_f=0.22 at 30% EtOAc/Hex, 340 mg, 1.18 mmol) Yield: 77%. ^{1}H NMR (500 MHz, $CDCl_3$) *δ* 4.42 (s, 1H), 4.33 – 4.15 (m, 1H), 3.87-3.70 (m, 5H), 1.57 (s, 3H), 1.52 (s, 3H), 1.45 (s, 9H). ^{3}C NMR (126 MHz, $CDCl_3$) δ 171.2, 153.3, 96.4, 81.6, 75.4, 64.2, 62.4, 52.7, 28.5, 28.3, 27.5

3-(4-methoxyphenoxy)propan-1-ol (19): 18 (1.37 g, 11 mmol) was converted to **19** according to general procedure G. After column chromatography purification using a gradient of 20%→50% EtOAc/Hex, a white solid was recovered (R_f= 0.42 at 40% EtOAc/Hex, 1.7 g, 9.35 mmol). Yield: 85%. ^{1}H NMR (250 MHz, $CDCl_3$) *δ* 6.83 (s, 4H), 4.07 (t, *J* = 5.9 Hz, 2H), 3.85 (t, *J* = 5.9 Hz, 2H), 3.76 (s, 3H), 2.09-1.95 (s, 2H). ^{13}C NMR (63 MHz, CDCl3) δ 154.1, 153.0, 115.6, 114.8, 66.7, 60.8, 55.9, 32.2

3-(4-methoxyphenoxy)propanal (20): 19 (1.60 g, 8.79 mmol) was converted to **20** according to general procedure H. After column chromatography purification using a gradient of 20%→30% EtOAc/Hex, a yellowish oil was recovered (R_f= 0.5 at 30% EtOAc/Hex, 1.27 g, 7.03 mmol). Yield: 80%. ^{1}H NMR (250 MHz, $CDCl_3$) δ 9.86 (t, J = 1.6 Hz, 1H), 6.84 (s, 4H), 4.26 (t, J = 6.1 Hz, 2H), 3.76 (s, 3H), 2.86 (td, J = 6.1, 1.6 Hz, 2H). ^{13}C NMR (63 MHz, $CDCl_3$) δ 200.5, 154.3, 152.7, 115.8, 115.8 114.8, 114.8, 62.6, 55.8, 43.5

(E)-methyl 5-(4-methoxyphenoxy)pent-2-enoate (21): 20 (1.15 g, 6.39 mmol) was converted to **21** according to general procedure A. After column chromatography purification using a gradient of 10%→30% EtOAc/Hex, a yellowish oil was recovered (R_f= 0.43 at 20% EtOAc/Hex, 1.0 g, 4.23 mmol). Yield: 66%. ^{1}H NMR (250 MHz, $CDCl_3$) δ 7.17 – 6.98 (m, 1H), 6.86 (s, 4H), 5.99 (d, *J* = 15.7 Hz, 1H), 4.05 (t, *J* = 6.3 Hz, 2H), 3.78 (d, *J* = 7.5 Hz, 6H), 2.69 (q, *J* = 7.2, 6.6 Hz, 2H). ^{13}C NMR (126 MHz, CDCl3) δ 166.9, 154.2, 152.8, 145.3, 123.1, 115.7, 114.8, 66.8, 55.8, 51.6, 32.3

(2S,3R)-methyl 3-((*tert*-butoxycarbonyl)amino)-2-hydroxy-5-(4-methoxyphenoxy)pentanoate (22): 21 (236 mg, 1 mmol) was converted to **22** according to the general procedure B. After column chromatography purification using a gradient of 20%→40% EtOAc/Hex a yellowish oil was recovered (R_f=0.28 at 30% EtOAc/Hex, 250 mg, 0.67 mmol). Yield: 67%. ^{1}H NMR (250 MHz, $CDCl_3$) δ 6.89-6.75 (m, 4H), 4.95 (d, *J* = 9.7 Hz, 1H), 4.37-4.26 (m, 2H), 3.98 (t, *J* = 6.2 Hz, 2H), 3.77 (s, 3H), 3.73 (s, 3H), 3.28 (s, 1H), 2.13-1.93 (m, 2H), 1.37 (s, 9H). $_{13}$C NMR (126 MHz, $CDCl_3$) δ 173.9, 155.5, 154.1, 153.0, 115.8, 115.8, 114.7, 114.7, 79.7, 72.4, 65.8, 55.8, 52.8, 50.8, 32.0, 28.3, 28.3, 28.3

***(4R,5S)*-3-*tert*-butyl 5-methyl 4-(2-(4-methoxyphenoxy)ethyl)-2,2-dimethyloxazolidine-3,5-dicarboxylate (23): 22** (395 mg, 1.07 mmol) was converted to **23** according to general procedure L. After column chromatography purification using a gradient of 10%→20% EtOAc/Hex, a yellowish oil was recovered (R_f= 0.4 at 20% EtOAc/Hex, 365 g, 0.89 mmol). Yield: 83%. ^{1}H NMR (250 MHz, $CDCl_3$) δ 6.80 (d, *J* = 1.6 Hz, 4H), 4.66 (s, 1H), 4.41 (d, *J* = 9.2 Hz, 1H), 4.01 (t, *J* = 5.8 Hz, 2H), 3.73 (s, *3*H), 3.70 (s, 3H) 2.44 – 2.20 (m, 1H), 2.19 – 2.04 (m, 1H), 1.58 (d, *J* = 10.8 Hz, 6H), 1.47 (s, 9H). ^{13}C NMR (63 MHz, $CDCl_3$) δ 171.6, 153.9, 152.8, 129.8, 128.0, 115.3, 115.3, 114.5, 114.5, 95.7, 80.5, 78.3, 65.8, 59.0, 52.4, 31.6, 28.4, 28.4, 28.4, 22.6, 22.6

(4R,5S)-3-*tert*-butyl 5-methyl 4-(2-hydroxyethyl)-2,2-dimethyloxazolidine-3,5-dicarboxylate (24): 23 (620 mg, 1.51 mmol) was dissolved in 15 mL CH_3CN at 0^0C. CAN (1.8 g, 3.3 mmol) was dissolved in 15 mL H_2O and was added dropwise in the reaction mixture. Reaction was stirred at 0^0C for 30 minutes, quenched with $Na_2S_2O_3$ and washed with EtOAc (×3). The combined organic layers were dried (Mg_2SO_4), filtered and concentrated under reduced pressure. Flash chromatographic purification using a gradient of 30%→40% EtOAc/Hex gave pure alcohol **13b** as a yellowish liquid (R_f=0.14 at 30% EtOAc/Hex, 370 mg, 1.22 mmol) Yield: 81%. ^{1}H NMR (250 MHz, MeOD) δ 4.59 (d, J = 2.2 Hz, 1H), 4.39-4.25 (br, 1H), 3.76 (s, 3H), 3.65 (t, J = 6.4 Hz, 2H), 2.10 – 1.76 (m, 2H), 1.55 (d, J = 3.7 Hz, 6H), 1.48 (s, 9H). ^{13}C NMR (63 MHz, CDCl3) δ 171.7, 153.1, 96.1, 81.4, 78.9, 58.8, 57.3, 52.5, 38.4, 28.4, 27.6

(S)-benzyl 2-((S)-2-((2S,3R)-3-amino-2,4-dihydroxybutanamido)-4-methylpentanamido)-3-(1H-indol-3-yl)propanoate (25): 17 (25 mg, 0.085 mmol) was converted to **25** according to general procedures C,D and F. After purification with column chromatography using a gradient of 5→10% MeOH/CH_2Cl_2 and was isolated as amorphous white solid (R_f= 0.32 at 10% MeOH / CH_2Cl_2, 21.0 mg, 0.04 mmol). Yield: 47%. ^{1}H NMR (250 MHz, MeOD) δ 7.51 (d, J = 7.7 Hz, 1H), 7.37 – 7.22 (m, 4H), 7.20 – 6.95 (m, 5H), 5.04 (s, 2H), 4.75 (dd, J = 6.9 Hz, J = 6.9 Hz, 1H), 4.44 (dd, J = 7.5 Hz, J = 7.5 Hz, 1H), 4.22 (dd, J = 3.7 Hz, J = 3.7 Hz, 1H), 3.71 (dd, J = 11.2, 5.2 Hz, 1H), 3.60 (dd, J = 10.8, 7.3 Hz, 1H), 3.34 – 3.28 (m, 1H), 3.21 (dd, J = 14.6, 7.5 Hz, 1H), 1.68 – 1.45 (m, 3H), 0.89 (d, J = 6.1 Hz, 3H), 0.87 (d, J = 6.0 Hz, 3H). ^{13}C NMR (63 MHz, MeOD) δ 174.5, 174.2, 173.2, 138.0, 136.9, 129.5, 129.3, 129.3, 128.6, 124.7, 122.4, 119.9, 119.1, 112.4, 110.4, 70.6, 68.1, 61.8, 56.3, 55.1, 53.0, 41.9, 28.4, 25.8, 23.3, 22.1. ESI HRMS: *m/z* [M + H]+ calcd for $C_{28}H_{39}N_4O_6^+$, 525.2708; found, 525.2700

(S)-benzyl 2-((S)-2-((2S,3R)-3-amino-2,5-dihydroxypentanamido)-4-methylpentanamido)-3-(1H-indol-3-yl)propanoate (26): 24 (31 mg, 0.099 mmol) was converted to **26** according to general procedures C,D and F. After purification with column chromatography using a gradient of 5→10% MeOH/CH_2Cl_2 and was isolated as amorphous yellowish solid (R_f= 0.30 at 10% MeOH / CH_2Cl_2, 15.0 mg, 0.02 mmol). Yield: 24%. ^{1}H NMR (250 MHz, MeOD) δ 7.70 – 6.84 (m, 10H), 5.04 (s, 2H), 4.75 (t, J = 6.9 Hz, 1H), 4.44 (t, J = 7.4 Hz, 1H), 4.19 (d, J = 4.2 Hz, 1H), 3.79 – 3.69 (m, 2H), 3.63 – 3.51 (m, 1H), 3.28 – 3.13 (m, 2H), 2.02 – 1.53 (m, 5H), 0.89 (t, J = 6.1 Hz, 6H). 13C NMR (63 MHz, MeOD) δ 174.4, 173.3, 173.1, 138.0, 136.94 129.5, 129.3, 129.3, 128.7, 124.7, 122.5, 119.9, 119.13 112.4, 110.4, 71.4, 68.1, 59.7, 55.1, 54.0, 53.0, 41.9, 32.6, 28.4, 25.8, 23.3, 22.1. ESI HRMS: *m/z* [M + H]+ calcd for $C_{29}H_{39}N_4O_6^+$, 539.2864; found, 539.2860

(4*S*,5*S*)-3-*tert*-butyl 5-methyl 4-formyl-2,2-dimethyloxazolidine-3,5-dicarboxylate (27a): 17 (383 mg, 1.32 mmol) was converted to **27a** according to general procedure H. After column chromatography purification using a gradient of 20%→40% EtOAc/Hex, a yellowish oil was recovered (R_f= 0.36 at 40% EtOAc/Hex, 340 mg, 1.22 mmol). Yield: 93%. ^{1}H NMR (250 MHz,

$CDCl_3$) δ 9.58 (s, 1H), 4.80 – 4.37 (m, 2H), 3.77 (s, 3H), 1.77 – 1.30 (m, 15H). ^{13}C NMR (63 MHz, $CDCl_3$) δ 196.7, 170.0, 150.8, 97.3, 81.7, 73.6, 73.2, 52.9, 28.2

***(4R,5S)*-3-*tert*-butyl 5-methyl 2,2-dimethyl-4-(2-oxoethyl)oxazolidine-3,5-dicarboxylate (27b): 24** (400 mg, 1.32 mmol) was converted to **27b** according to general procedure H. After column chromatography purification using a gradient of 20%→40% EtOAc/Hex, a yellowish oil was recovered (R_f= 0.37 at 40% EtOAc/Hex, 340 mg, 1.13 mmol). Yield: 85%. ^1H NMR (250 MHz, $CDCl_3$) δ 9.76 (s, 1H), 4.74 – 4.56 (m, 1H), 4.34 (d, J = 3.4 Hz, 1H), 3.78 (s, 3H), 3.11-2.87 (m, 1H), 2.76 (dd, J = 16.8, 7.7 Hz, 1H), 1.62 – 1.36 (m, 15H). ^{13}C NMR (63 MHz, $CDCl_3$) δ 199.5, 170.8, 151.7, 96.0, 81.2, 78.0, 55.2, 52.7, 47.1, 28.4, 28.4, 28.4, 27.2, 27.2

Methyl 2-(2-(3-amino-2,7-dihydroxyheptanamido)-4-methylpentanamido)-3-(4-hydroxyphenyl) propanoate (30): 27b (30 mg, 0.1 mmol) was converted to **30** according to general procedures A, C, E, D and F and was isolated as white amorphous solid (5.7 mg, 0.012 mmol). Yield : 12 %; ^1H NMR (250 MHz, MeOD) δ 7.04 (d, J = 8.3 Hz, 2H), 6.71 (d, J = 8.4 Hz, 2H), 4.67 – 4.54 (m, 1H), 4.54 – 4.38 (m, 1H), 4.26 (dd, J = 25.5, 3.3 Hz, 1H), 3.71 (s, 3H), 3.61 (t, J = 6.1 Hz, 2H), 3.08 (dd, J = 14.0, 5.5 Hz, 1H), 2.99-2.83 (m, 1H), 2.54-2.37 (m, 1H), 2.00 – 1.74 (m, 3H), 1.66 – 1.43 (m, 6H), 1.09 – 0.89 (m, 6H). ^{13}C NMR (63 MHz, MeOD) δ 174.2, 173.4, 173.1, 157.4, 131.3, 128.7, 116.3, 70.7, 62.3, 55.5, 55.0, 53.1, 52.7, 42.0, 37.5, 33.0, 30.2, 25.9, 23.2, 22.8, 22.3. ESI HRMS: *m/z* [M + H]+ calcd for $C_{23}H_{38}N_3O_7^+$, 468.2705; found, 468.2723

(S)-methyl 2-((S)-2-((2S,3R)-3-amino-5-(4-(benzyloxy)phenoxy)-2-hydroxypentanamido)-4-methyl pentanamido)-3-(4-hydroxyphenyl)propanoate (32a): 24 (25 mg, 0.083 mmol) was converted to **32a** (20.6 mg, 0.033mmol) according to general procedures G, C, D and F. After purification with column chromatography using a gradient of 5→10% MeOH/CH_2Cl_2 and was isolated as yellow oil (R_f= 0.24 at 5% MeOH / CH_2Cl_2, 17 mg, 0.027 mmol). Yield: 40 %. ^1H NMR (500 MHz, Acetic) δ 7.41 (d, J = 7.3 Hz, 2H), 7.35 (dd, J = 7.5 Hz, 2H), 7.29 (t, J = 7.3 Hz, 1H), 7.00 (d, J = 8.5 Hz, 2H), 6.92 (d, J = 9.3 Hz, 2H), 6.88 (d, J = 9.3 Hz, 2H), 6.76 (d, J = 8.5 Hz, 2H), 5.04 (s, 2H), 4.82 (dd, J = 7.9, 5.5 Hz, 1H), 4.64 (d, J = 4.8 Hz, 1H), 4.63 – 4.58 (m, 1H), 4.19 – 4.10 (m, 2H), 4.01 – 3.96 (m, 1H), 3.72 (s, 3H), 3.10 (dd, J = 14.1, 5.4 Hz, 1H), 2.93 (dd, J = 14.1, 8.0 Hz, 1H), 2.33 – 2.26 (m, 1H), 2.21 – 2.13 (m, 1H), 1.68 – 1.54 (m, 3H), 0.91 (d, J = 5.9 Hz, 3H), 0.87 (d, J = 6.0 Hz, 3H). ^{13}C NMR (126 MHz, D_2O) δ 174.1, 173.4, 173.4, 156.5, 154.5, 153.7, 138.6, 131.4, 129.4, 128.7, 128.4, 128.3, 117.0, 116.6, 116.4, 71.3, 70.7, 66.5, 55.0, 54.1, 53.1, 53.0, 41.3, 37.4, 29.3, 25.5, 23.1, 22.0. ESI HRMS: *m/z* [M + H]+ calcd for $C_{34}H_{44}N_3O_8^+$, 622.3123; found, 622.3148

(S)-benzyl 2-((S)-2-((2S,3R)-3-amino-5-(4-(benzyloxy)phenoxy)-2-hydroxypentanamido)-4-methyl pentanamido)-3-(1H-indol-3-yl)propanoate (32b): 24 (25 mg, 0.083 mmol) was converted to **32b** (20.6 mg, 0.033mmol) according to general procedures G, C, D and F. After purification with column chromatography using a gradient of 5→10% MeOH/CH_2Cl_2 and was isolated as amorphous yellow solid (R_f= 0.35 at 5% MeOH / CH_2Cl_2, 18.6 mg, 0.029 mmol). Yield: 35 %. ^{1}H NMR (500 MHz, Acetic Acid-*d*$_4$) *δ* 7.51 (d, *J* = 7.9 Hz, 1H), 7.40 (d, *J* = 7.1 Hz, 2H), 7.37 – 7.26 (m, 7H), 7.24 – 7.20 (m, 2H), 7.14 – 7.08 (m, 1H), 7.06 (s, 1H), 7.05 – 7.01 (m, 1H), 6.91 (d, *J* = 9.2 Hz, 2H), 6.86 (d, *J* = 9.2 Hz, 2H), 5.09 (s, 2H), 5.03 (s, 2H), 4.95 (t, *J* = 6.4 Hz, 1H), 4.63 – 4.57 (m, 2H), 4.14 – 4.03 (m, 2H), 3.99 – 3.89 (m, 1H), 3.35 (dd, *J* = 14.9, 5.9 Hz, 1H), 3.28 (dd, *J* = 14.9, 7.0 Hz, 1H), 2.31 – 2.20 (m, 1H), 2.19 – 2.09 (m, 1H), 1.67 – 1.50 (m, 3H), 0.85 (d, *J* = 5.9 Hz, 3H), 0.82 (d, *J* = 5.9 Hz, 3H). ^{13}C NMR (126 MHz, D_2O) δ 174.1, 173.4, 173.1, 154.4, 153.7, 138.6, 137.5, 136.5, 129.5, 129.4, 129.3, 128.7, 128.5, 128.4, 124.6, 122.7, 120.2, 119.3, 116.9, 116.6, 112.4, 110.0, 71.3, 70.8, 68.4, 66.4, 54.6, 54.0, 53.0, 41.2, 29.3, 28.2, 25.5, 23.1, 22.0. ESI HRMS: *m/z* [M + H]+ calcd for $C_{42}H_{49}N_4O_7^+$, 721.3596; found, 721.3623

(S)-methyl 2-((S)-2-((2S,3R)-3-amino-2-hydroxy-5-(4-hydroxyphenoxy)pentanamido)-4-methyl pentanamido)-3-(4-hydroxyphenyl)propanoate (32c): 32a (12 mg, 0.019 mmol) was converted to **32c** according to general procedure E. After purification with column chromatography using a gradient of 10→20% MeOH/CH_2Cl_2 and was isolated as amorphous white solid (R_f= 0.24 at 10% MeOH / CH_2Cl_2, 6 mg, 0.011 mmol). Yield: 58 %. ^{1}H NMR (250 MHz, Acetic Acid-*d*$_4$) δ 7.00 (d, *J* = 8.5 Hz, 2H), 6.87 – 6.72 (m, 6 H), 4.82 (dd, *J* = 8.0, 5.3 Hz, 1H), 4.66 (d, *J* = 4.7 Hz, 1H), 4.65 – 4.54 (m, 1H), 4.20 – 4.10 (m, 2H), 4.05 – 3.94 (m, 1H), 3.72 (s, 3H), 3.11 (dd, *J* = 14.1, 5.3 Hz, 1H), 2.92 (dd, *J* = 14.0, 8.1 Hz, 1H), 2.35 – 2.12 (m, 2H), 1.73 – 1.49 (m, 3H), 0.91 (d, *J* = 5.9 Hz, 3H), 0.87 (d, *J* = 5.6 Hz, 3H). ^{13}C NMR (63 MHz, Acetic) *δ* 174.1, 173.4, 173.4, 156.5, 153.0, 151.8, 131.4, 128.3, 116.9, 116.8, 116.3, 70.7, 66.7, 54.9, 54.3, 53.1, 53.0, 41.2, 37.4, 29.1, 25.5, 23.1, 22.0. ESI HRMS: *m/z* [M + H]+ calcd for $C_{27}H_{38}N_3O_8^+$, 532.2653; found, 532.2677

(S)-methyl 2-((S)-2-((2S,3R)-3-amino-2-hydroxy-5-(4-hydroxyphenoxy)pentanamido)-4-methylpentanamido)-3-(1H-indol-3-yl)propanoate (32d):): 24 (25 mg, 0.083 mmol) was converted to **32d** according to general procedures G, C, D, E and F. After purification with column chromatography using a gradient of 5→15% MeOH/CH_2Cl_2 and was isolated as amorphous white solid (R_f= 0.5 at 10% MeOH / CH_2Cl_2, 16 mg, 0.028 mmol). Yield: 34 %. ^{1}H NMR (500 MHz, MeOD) *δ* 7.53 – 7.49 (m, 1H), 7.34 – 7.29 (m, 1H), 7.13 – 7.05 (m, 2H), 7.03 – 6.98 (m, 1H), 6.83 – 6.78 (m, 1H), 6.82 – 6.74 (m, 1H), 6.73 – 6.69 (m, 2H), 4.72 (dd, *J* = 7.6, 5.7 Hz, 1H), 4.47 – 4.42 (m, 1H), 4.26 (d, *J* = 4.2 Hz, 1H), 4.10 – 4.00 (m, 2H), 3.74 – 3.69 (m, 1H), 3.64 (s, 3H), 3.34 – 3.27 (m, 1H), 3.20 (dd, *J* = 14.7, 7.7 Hz, 1H), 2.27 – 2.15 (m, 1H), 2.09 – 1.99 (m, 1H), 1.69 – 1.48 (m, 3H), 0.94 (d, *J* = 6.4 Hz, 3H), 0.91 (d, *J* = 6.4 Hz, 3H). ^{13}C NMR (63 MHz, MeOD) *δ* 174.4, 173.7, 173.2, 153.1, 152.9, 138.0, 128.7, 124.6, 122.5, 119.9, 119.1, 116.8, 116.8, 112.3, 110.5, 71.3, 66.1, 55.0, 53.2, 53.1, 52.7, 41.9, 30.5, 28.3, 25.9, 23.3, 22.2. ESI HRMS: *m/z* [M + H]+ calcd for $C_{29}H_{39}N_4O_7^+$, 555.2813; found, 555.2812

(S)-methyl 2-((S)-2-((2S,3R)-3-amino-2-hydroxy-4-(4-hydroxyphenoxy)butanamido)-4-methyl pentanamido)-3-(1H-indol-3-yl)propanoate (32e): 17 (25 mg, 0.085 mmol) was converted to **32e** according to general procedures G, C, D, E and F. After purification with column chromatography using a gradient of 5→15% MeOH/CH_2Cl_2 and was isolated as amorphous white solid (R_f= 0.45 at 10% MeOH / CH_2Cl_2, 9.2 mg, 0.017 mmol). Yield: 20 %. ^{1}H NMR (250 MHz, MeOD) δ 7.51 (d, J = 7.6 Hz, 1H), 7.32 (d, J = 8.1 Hz, 1H), 7.14 – 6.96 (m, 3H), 6.83 – 6.65 (m, 4H), 4.71 (dd, J = 7.4, 6.0 Hz, 1H), 4.47 (t, J = 7.2 Hz, 1H), 4.25 (d, J = 3.6 Hz, 1H), 3.96 (dd, J = 9.4, 6.3 Hz, 1H), 3.84 (dd, J = 9.4, 6.5 Hz, 1H), 3.64 (s, 3H), 3.48 – 3.39 (m, 1H), 3.36 – 3.25 (m, 1H), 3.19 (dd, J = 14.7, 7.8 Hz, 1H), 1.70 – 1.50 (m, 3H), 0.93 (d, J = 6.3 Hz, 3H), 0.90 (d, J = 6.3 Hz, 3H).^{13}C NMR (63 MHz, MeOD) δ 174.9, 174.5, 173.8, 153.3, 152.7, 138.0, 128.7, 124.6, 122.4, 119.9, 119.1, 116.8, 116.8, 112.3, 110.5, 71.8, 70.0, 54.9, 54.3, 52.9, 52.7, 41.9, 28.3, 25.9, 23.3, 22.2. ESI HRMS: *m/z* [M + H]+ calcd for $C_{28}H_{37}N_4O_7^+$, 541.2657; found, 541.2644

(S)-2-((S)-2-((2S,3R)-3-amino-2-hydroxy-5-(4-hydroxyphenoxy)pentanamido)-4-methylpentanamido)-3-(1H-indol-3-yl)propanoic acid (32f): 32b (20 mg, 0.028 mmol) was converted to **32f** according to general procedure E. After purification with column chromatography using a gradient of 10→20% MeOH/CH_2Cl_2 and was isolated as black-red amorphous solid (R_f= 0.3 at 20% MeOH / CH_2Cl_2, 10 mg, 0.018 mmol). Yield: 68 %. ^{1}H NMR (500 MHz, Acetic Acid-d_4) δ 7.57 (d, J = 7.9 Hz, 1H), 7.34 (d, J = 8.1 Hz, 1H), 7.15 (s, 1H), 7.10 (dd, J = 7.3 Hz, 1H), 7.03 (dd, J = 7.4 Hz, 1H), 6.82 – 6.76 (m, 4H), 4.93 (dd, J = 7.4, 5.0 Hz, 1H), 4.67 – 4.56 (m, 2H), 4.14 – 4.01 (m, 2H), 3.97 – 3.88 (m, 1H), 3.40 (dd, J = 15.0, 5.1 Hz, 1H), 3.30 (dd, J = 14.9, 7.5 Hz, 1H), 2.27 – 2.20 (m, 1H), 2.16 – 2.08 (m, 1H), 1.69 – 1.56 (m, 3H), 0.89 (d, J = 5.7 Hz, 3H), 0.85 (d, J = 5.8 Hz, 3H). ^{13}C NMR (63 MHz, Acetic) δ 176.9, 174.1, 173.5, 153.0, 151.8, 137.5, 128.5, 124.7, 122.6, 120.1, 119.3, 116.9, 116.7, 112.3, 110.0, 70.7, 66.5, 54.1, 53.0, 41.1, 30.6, 29.1, 28.0, 25.5, 23.1, 21.9. ESI HRMS: *m/z* [M + H]+ calcd for $C_{28}H_{37}N_4O_7^+$, 541.2657; found, 541.2646

(S)-methyl 2-((S)-2-((2S,3R)-3-amino-2-hydroxy-5-(3-hydroxyphenoxy)pentanamido)-4-methyl pentanamido)-3-(4-hydroxyphenyl)propanoate (32g): 24 (20 mg, 0.066 mmol) was converted to **32g** according to general procedures G, C, D, E and F. After purification with column chromatography using a gradient of 5→10% MeOH/CH_2Cl_2 and was isolated as yellow amorphous solid (R_f= 0.34 at 10% MeOH / CH_2Cl_2, 5 mg, 0.009 mmol). Yield: 13.6 %. ^{1}H NMR (250 MHz, Acetic Acid-d_4) δ 7.19 – 6.92 (m, 3H), 6.77 (d, J = 8.2 Hz, 2H), 6.60 – 6.36 (m, 3H), 4.82 (dd, J = 8.1, 5.2 Hz, 1H), 4.74 – 4.44 (m, 2H), 4.30 – 4.07 (m, 2H), 3.98 (dt, J = 9.2, 4.6 Hz, 1H), 3.72 (s, 3H), 3.20 – 2.82 (m, 2H), 2.40 – 2.15 (m, 2H), 1.71 – 1.56 (m, 3H), 0.97 – 0.84 (m, 6H). ^{13}C NMR (63 MHz, Acetic) δ 174.1, 173.4, 173.3, 160.6, 158.7, 156.5, 131.4, 130.9, 128.3, 116.3, 109.4, 107.2, 103.2, 70.7, 65.7, 54.9, 54.0, 53.1, 53.0, 41.2, 37.4, 30.6, 25.5, 23.1, 22.0. ESI HRMS: *m/z* [M + H]+ calcd for $C_{27}H_{38}N_3O_8^+$, 532.2654; found, 532.2678

(S)-2-((S)-2-((2S,3R)-3-amino-2-hydroxy-5-(3-hydroxyphenoxy)pentanamido)-4-methylpentanamido)-3-(1H-indol-3-yl)propanoic acid (32h): 24 (35 mg, 0.116 mmol) was converted to **32h** according to general procedures G, C, D, E and F. After purification with column chromatography using a gradient of 5→10% MeOH/CH_2Cl_2 and was isolated as brown-pink amorphous solid (R_f= 0.34 at 20% MeOH / CH_2Cl_2, 30 mg, 0.055 mmol). Yield: 47 %. ^{1}H NMR (250 MHz, Acetic Acid-*d*$_4$) δ 7.57 (d, *J* = 7.6 Hz, 1H), 7.34 (d, *J* = 7.9 Hz, 1H), 7.21 – 6.93 (m, 4H), 6.51 – 6.29 (m, 3H), 4.94 (dd, *J* = 7.3, 5.0 Hz, 1H), 4.67 – 4.57 (m, 2H), 4.19 – 4.05 (m, 2H), 4.02 – 3.90 (m, 1H), 3.39 (dd, *J* = 15.0, 4.7 Hz, 1H), 3.29 (dd, *J* = 15.0, 7.3 Hz, 1H), 2.37 – 2.10 (m, 2H), 1.71 – 1.53 (m, 3H), 0.89 (d, *J* = 5.6 Hz, 3H), 0.85 (d, *J* = 5.6 Hz, 3H). ^{13}C NMR (63 MHz, Acetic) δ 176.8, 174.2, 173.4, 160.5, 158.7, 137.4, 130.9, 128.5, 124.7, 122.6, 120.1, 119.3, 112.3, 110.0, 109.4, 107.1, 103.2, 70.7, 65.6, 54.2, 54.0, 53.0, 41.1, 29.0, 28.0, 25.5, 23.1, 21.9. ESI HRMS: *m/z* [M + H]+ calcd for $C_{28}H_{37}N_4O_7^+$, 541.2657; found, 541.2681

(S)-methyl 2-((S)-2-((2S,3R)-3-amino-2-hydroxy-5-(2-hydroxyphenoxy)pentanamido)-4-methyl pentanamido)-3-(4-hydroxyphenyl)propanoate (32i): 24 (25 mg, 0.083 mmol) was converted to **32i** according to general procedures G, C, D, E and F. After purification with column chromatography using a gradient of 5→10% MeOH/CH_2Cl_2 and was isolated as white amorphous solid (R_f= 0.27 at 10% MeOH / CH_2Cl_2, 17.6 mg, 0.033 mmol). Yield: 40 %. ^{1}H NMR (250 MHz, Acetic Acid-*d*$_4$) δ 6.99 (d, *J* = 8.3 Hz, 2H), 6.96 – 6.80 (m, 4H), 6.76 (d, *J* = 8.3 Hz, 2H), 4.82 (dd, *J* = 8.0, 5.3 Hz, 1H), 4.71 – 4.55 (m, 2H), 4.33 – 4.15 (m, 2H), 4.09 – 3.96 (m, 1H), 3.72 (s, 3H), 3.10 (dd, *J* = 14.0, 5.4 Hz, 1H), 2.91 (dd, *J* = 14.0, 8.0 Hz, 1H), 2.41 – 2.12 (m, 2H), 1.73 – 1.50 (m, 3H), 0.92 (d, *J* = 5.7 Hz, 3H), 0.88 (d, *J* = 5.7 Hz, 3H). ^{13}C NMR (63 MHz, Acetic) δ 174.0, 173.5, 173.3, 156.5, 147.3, 147.1, 131.4, 128.3, 123.2, 121.2, 116.7, 116.3, 114.5, 70.9, 67.7, 55.0, 54.7, 53.1, 53.0, 41.3, 37.5, 29.0, 25.5, 23.1, 22.01. ESI HRMS: *m/z* [M + H]+ calcd for $C_{27}H_{38}N_3O_8^+$, 532.2654; found, 532.2674

(S)-2-((S)-2-((2S,3R)-3-amino-2-hydroxy-5-(2-hydroxyphenoxy)pentanamido)-4-methylpentanamido)-3-(1H-indol-3-yl)propanoic acid (32j): 24 (25 mg, 0.083 mmol) was converted to **32j** according to general procedures G, C, D, E and F. After purification with column chromatography using a gradient of 5→10% MeOH/CH_2Cl_2 and was isolated as brown-pink amorphous solid (R_f= 0.39 at 10% MeOH / CH_2Cl_2, 10.0 mg, 0.033 mmol). Yield: 40 %. ^{1}H NMR

(250 MHz, Acetic Acid-d_4) δ 7.56 (d, J = 7.6 Hz, 1H), 7.33 (d, J = 7.8 Hz, 1H), 7.16 – 6.98 (m, 3H), 6.95 – 6.75 (m, 4H), 4.94 (dd, J = 7.3, 5.0 Hz, 1H), 4.73 – 4.51 (m, 2H), 4.31 – 4.07 (m, 2H), 4.06 – 3.90 (m, 1H), 3.40 (dd, J = 15.0, 5.1 Hz, 1H), 3.28 (dd, J = 15.0, 7.3 Hz, 1H), 2.42 – 2.11 (m, 2H), 1.75 – 1.54 (m, 3H), 0.89 (d, J = 5.5 Hz, 3H), 0.85 (d, J = 5.5 Hz, 3H). ^{13}C NMR (63 MHz, Acetic) δ 176.9, 174.1, 173.4, 147.3, 147.1, 137.5, 128.5, 124.7, 123.2, 122.7, 121.2, 120.1, 119.3, 116.7, 114.5, 112.3, 110.1, 70.9, 67.7, 54.7, 54.2, 53.1, 41.1, 29.0, 28.0, 25.5, 23.1, 21.9. ESI HRMS: *m/z* [M + H]+ calcd for $C_{28}H_{37}N_4O_7^+$, 541.2657; found, 541.2680

(S)-methyl 2-((S)-2-((2S,3R)-3-amino-5-(3-chlorophenoxy)-2-hydroxypentanamido)-4-methyl pentanamido)-3-(1H-indol-3-yl)propanoate (32k): 24b (39 mg, 0.13 mmol) was converted to **32k** according to general procedures G, C, D and F. After column chromatography purification using 10% MeOH/CH_2Cl_2 a white solid was recovered (R_f= 0,4 10% MeOH/CH_2Cl_2 (29 mg, 0.05 mmol). Yield: 38 %, ^{1}H NMR (500 MHz, CD_3OD) δ 7.51 (d, J = 7.9 Hz, 1H), 7.32 (d, J = 8.1 Hz, 1H), 7.24 (t, J = 8.2 Hz, 1H), 7.16 – 7.05 (m, 2H), 7.04 – 6.93 (m, 3H), 6.88 (dd, J = 8.0, 2.1 Hz, 1H), 4.78 – 4.67 (m, 1H), 4.44 (t, J = 7.5 Hz, 1H), 4.27 (d, J = 4.3 Hz, 1H), 4.18-4.04 (m, 2H), 3.75-3.68 (m, 1H), 3.64 (s, 3H), 3.29 (d, J = 5.8 Hz, 1H), 3.20 (dd, J = 14.7, 7.6 Hz, 1H), 2.30 – 2.20 (m, 1H), 2.12-2.02 (m, 1H), 1.71 – 1.55 (m, 3H), 0.92 (dd, J = 13.1, 6.4 Hz, 6H). ^{13}C NMR (126 MHz, CD_3OD) δ 174.3, 173.7, 173.0, 160.7, 138.0, 135.9, 131.6, 128.68, 124.6, 122.4, 119.9, 119.1, 116.1, 114.2, 112.3, 110.5, 106.9, 71.0, 65.5, 54.9, 53.2, 53.0, 52.7, 41.8, 30.1, 28.3, 25.9, 23.2, 22.2. ESI HRMS: *m/z* [M + H]+ calcd for $C_{29}H_{38}ClN_4O_6^+$, 573.2474; found, 573.2466

(S)-methyl 2-((S)-2-((2S,3R)-3-amino-5-(2-chlorophenoxy)-2-hydroxypentanamido)-4-methyl pentanamido)-3-(4-hydroxyphenyl)propanoate (32l): 24 (20 mg, 0.066 mmol) was converted to **32l** according to general procedures G, C, D and F. After column chromatography purification using 10% MeOH/CH_2Cl_2 a brown amorphous solid was recovered (7.7 mg, 0.014 mmol). Yield: 38 %; ^{1}H NMR (500 MHz, MeOD) δ 7.27 (t, J = 8.1 Hz, 1H), 7.06 – 6.86 (m, 5H), 6.75 – 6.62 (m, 2H), 4.64 – 4.52 (m, 1H), 4.51-4.40 (m, 1H), 4.37 (d, J = 2.8 Hz, 1H), 4.25 – 3.98 (m, 2H), 3.69 (s, 3H), 3.06 (dd, J = 14.0, 5.4 Hz, 1H), 2.88 (dd, J = 14.0, 8.9 Hz, 1H), 2.49 – 2.45 (m, 1H), 2.39-2.36 (m, 1H), 2.35-2.29 (m, 1H), 1.67 – 1.46 (m, 3H), 0.94 (dd, J = 17.4, 6.1 Hz, 6H). ^{13}C NMR (63 MHz, MeOD) δ 174.1, 173.4, 172.3, 160.5 157.4, 136.1, 131.8, 131.3, 128.7, 122.47, 116.3, 115.8, 114.2, 106.9, 73.0, 65.2, 60.0, 52.7, 55.6, 52.6, 42.2, 37.5, 30.8, 26.0, 23.4, 21.9. ESI HRMS: *m/z* [M + H]+ calcd for $C_{27}H_{37}ClN_3O_7^+$, 550.2315; found, 550.2314

Methyl 2-((S)-2-((2S,3R)-3-amino-2-hydroxy-4-(3,4,5-trifluorophenoxy)butanamido)-4-methyl pentanamido)-3-(1H-indol-3-yl)propanoate (32m): 17 (30 mg, 0.1 mmol) was converted to **32m** according to general procedures G, C, D and F. After purification with column chromatography using a gradient of 5→10% MeOH/CH_2Cl_2 and was isolated as brownish amorphous solid (R_f= 0.32 at 10% MeOH / CH_2Cl_2, 11.0 mg, 0.017 mmol). Yield: 17 %. ^{1}H NMR (250 MHz, Methanol-*d*$_4$) δ 7.59 – 7.40 (m, 1H), 7.36 – 7.24 (m, 1H), 7.17 – 6.91 (m, 3H), 6.77 – 6.65 (m, 2H), 4.72 (t, *J* = 5.8 Hz, 1H), 4.47 (t, *J* = 7.4 Hz, 1H), 4.18 (d, *J* = 3.6 Hz, 1H), 4.02 – 3.75 (m, 2H), 3.64 (s, 3H), 3.43 – 3.34 (m, 1H), 3.29 – 3.11 (m, 2H), 1.64 – 1.48 (m, 3H), 0.95 – 0.87 (m, 6H).^{13}C NMR (63 MHz, MeOD) δ 174.8, 174.4, 173.8, 155.8 (td, *J* = 12, 3 Hz), 152.7 (ddd, J = 245.9, 11, 6 Hz, 2C), 138.0, 135.8 (t, *J* = 241.92, 16 Hz, 1C), 128.7, 124.6, 122.4, 119.8, 119.1, 112.3, 110.5, 100.6 (m, 2C), 72.1, 70.8, 54.9, 54.0, 52.9, 52.7, 41.9, 28.4, 25.9, 23.3, 22.2. ESI HRMS: *m/z* [M + H]+ calcd for $C_{28}H_{34}F_3N_4O_6^+$, 579.2425; found, 579.2444

(4R,5S)-4-amino-6-(((S)-1-(((S)-1-(benzyloxy)-3-(1H-indol-3-yl)-1-oxopropan-2-yl)amino)-4-methyl-1-oxopentan-2-yl)amino)-5-hydroxy-6-oxohexanoic acid (34a): 17 (30 mg, 0.1 mmol) was converted to **34a** according to general procedures H, I, E, C, D and F. After purification with column chromatography using a gradient of 5→40% MeOH/CH_2Cl_2 and was isolated as amorphous white solid (R_f= 0.32 at 20% MeOH / CH_2Cl_2, 35.0 mg, 0.062 mmol). Yield: 62 %. ^{1}H NMR (500 MHz, D_2O) δ 7.50 (d, *J* = 7.7 Hz, 1H), 7.34 (d, *J* = 8.1 Hz, 1H), 7.28 (s, 3H), 7.16 (d, *J* = 4.0 Hz, 2H), 7.08 (t, *J* = 7.4 Hz, 1H), 7.04 (s, 1H), 7.00 (t, *J* = 7.4 Hz, 1H), 5.02 (d, *J* = 13.5 Hz, 2H), 4.76 (t, *J* = 6.7 Hz, 1H), 4.42 (t, *J* = 7.4 Hz, 1H), 4.25 (s, 1H), 3.54 (s, 1H), 3.35 – 3.27 (m, 1H), 3.22 (dd, *J* = 14.5, 7.6 Hz, 1H), 2.50 (bs, 2H), 2.07 – 1.94 (m, 1H), 1.94 – 1.84 (m, 1H), 1.62 – 1.42 (m, 3H), 0.87 (d, *J* = 6.3 Hz, 3H), 0.84 (d, *J* = 6.3 Hz, 3H).^{13}C NMR (126 MHz, DMSO) δ 174.4, 174.3, 173.3, 173.2, 138.0, 136.8, 129.5, 129.3, 128.6, 124.7, 122.4, 119.9, 119.1, 112.4, 110.3, 70.7, 68.1, 55.0, 54.9, 53.2, 41.7, 32.2, 28.3, 25.8, 25.8, 23.1, 22.1. ESI HRMS: *m/z* [M + H]+ calcd for $C_{30}H_{39}N_4O_7^+$, 567.2813; found, 567.2838

(4R,5S)-4-amino-6-(((S)-1-(((S)-1-carboxy-2-(1H-indol-3-yl)ethyl)amino)-4-methyl-1-oxopentan-2-yl)amino)-5-hydroxy-6-oxohexanoic acid (34b): 34a (15 mg, 0.027 mmol) was converted to **34b** according to general procedure E and was isolated as amorphous white solid (13.0 mg, 0.027 mmol). Yield: 100 %. ^{1}H NMR (500 MHz, D_2O) δ 7.56 (d, *J* = 7.7 Hz, 1H), 7.32 (d, *J* = 8.1 Hz, 1H), 7.12 (s, 1H), 7.07 (dd, *J* = 7.4 Hz, 1H), 7.00 (dd, *J* = 7.3 Hz, 1H), 4.69 – 4.65 (m, 1H), 4.39 (dd, *J* = 7.3 Hz, 1H), 4.22 (d, *J* = 3.3 Hz, 1H), 3.52 (d, *J* = 3.3 Hz, 1H), 3.40 – 3.30 (m, 1H), 3.20 (dd, *J* = 14.6, 7.7 Hz, 1H), 2.50 (t, *J* = 6.6 Hz, 2H), 2.06 – 1.98 (m, 1H), 1.94 – 1.85 (m, 1H), 1.64 – 1.49 (m, 3H), 0.91 (d, *J* = 6.2 Hz, 3H), 0.88 (d, *J* = 6.2 Hz, 3H). ^{13}C NMR (63 MHz, MeOD) δ 177.0, 176.3, 174.1, 173.3, 137.9, 128.9, 124.6, 122.3, 119.7, 119.3, 112.2, 111.0, 70.6, 55.2, 54.6, 53.4, 41.7, 31.4, 28.4, 25.8, 23.2, 22.1. ESI HRMS: *m/z* [M + H]+ calcd for $C_{23}H_{33}N_4O_7^+$, 477.2344; found, 477.2364

(5R,6S)-5-amino-7-(((S)-1-(((S)-1-(benzyloxy)-3-(1H-indol-3-yl)-1-oxopropan-2-yl)amino)-4-methyl-1-oxopentan-2-yl)amino)-6-hydroxy-7-oxoheptanoic acid (34c): 24 (30 mg, 0.1 mmol) was converted to **34c** according to general procedures H, I, E, C, D and F. After purification with column chromatography using a gradient of 10→20% MeOH/CH_2Cl_2 and was isolated as amorphous white solid (R_f= 0.56 at 20% MeOH / CH_2Cl_2, 10.1 mg, 0.017 mmol). Yield: 17 %. ^{1}H NMR (250 MHz, Acetic Acid-*d*$_4$) δ 7.51 (d, *J* = 7.7 Hz, 1H), 7.41 – 7.28 (m, 4H), 7.22 (dd, *J* = 6.7, 3.0 Hz, 2H), 7.17 – 7.08 (m, 1H), 7.08 – 6.99 (m, 2H), 5.10 (s, 2H), 4.94 (dd, *J* = 6.4 Hz, 1H), 4.63 – 4.54 (m, 1H), 4.50 (d, *J* = 4.3 Hz, 1H), 3.74 – 3.63 (m, 1H), 3.44 – 3.19 (m, 2H), 2.45 – 2.33 (m, 2H), 1.90 – 1.66 (m, 4H), 1.66 – 1.47 (m, 3H), 0.86 (d, *J* = 5.7 Hz, 3H), 0.82 (d, *J* = 5.7 Hz, 3H). ^{13}C NMR (63 MHz, Acetic) *δ* 179.5, 174.2, 173.5, 173.1, 137.5, 136.4, 129.5, 129.3, 128.4, 124.6, 122.7, 120.2, 119.2, 112.4, 109.9, 70.4, 68.4, 55.0, 54.6, 52.9, 41.2, 33.9, 29.0, 28.1, 25.4, 23.0. 22.0, 21.2. ESI HRMS: *m/z* [M + H]+ calcd for $C_{31}H_{41}N_4O_7^+$, 581.297; found, 581.2993

(5R,6S)-5-amino-6-hydroxy-7-(((S)-1-(((S)-3-(4-hydroxyphenyl)-1-methoxy-1-oxopropan-2-yl)amino)-4-methyl-1-oxopentan-2-yl)amino)-7-oxoheptanoic acid (34d): 24 (30 mg, 0.1 mmol) was converted to **34d** according to general procedures H, I, E, C, D and F. After purification with column chromatography using a gradient of 10→20% MeOH/CH_2Cl_2 and was isolated as amorphous white solid (R_f= 0.58 at 20% MeOH / CH_2Cl_2, 10.0 mg, 0.02 mmol). Yield: 20 %. ^{1}H NMR (250 MHz, Acetic Acid-*d*$_4$) *δ* 7.00 (d, *J* = 8.1 Hz, 2H), 6.76 (d, *J* = 8.1 Hz, 2H), 4.81 (dd, *J* = 7.9, 5.2 Hz, 1H), 4.59 (dd, *J* = 7.0 Hz, 1H), 4.51 (d, *J* = 4.2 Hz, 1H), 3.73 (s, 3H), 3.72 – 3.59 (m, 1H), 3.10 (dd, *J* = 14.1, 5.4 Hz, 1H), 2.93 (dd, *J* = 14.1, 8.0 Hz, 1H), 2.47 – 2.36 (m, 2H), 1.91 – 1.69 (m, 4H), 1.67 – 1.54 (m, 3H), 0.92 (d, *J* = 5.4 Hz, 3H), 0.87 (d, *J* = 5.4 Hz, 3H).^{13}C NMR (63 MHz, Acetic) *δ* 179.5, 174.1, 173.4, 173.4, 156.5, 131.4, 128.3, 116.3, 70.4, 55.0, 54.9, 53.1, 52.9, 41.2, 37.3, 33.9, 29.1, 25.5, 23.0, 22.0, 21.2. ESI HRMS: *m/z* [M + H]+ calcd for $C_{23}H_{36}N_3O_8^+$, 482.2497; found, 482.2498

2-((4*R*,5*S*)-3-(*tert*-butoxycarbonyl)-5-(methoxycarbonyl)-2,2-dimethyloxazolidin-4-yl)acetic acid (35): 24 (190 mg, 0.63 mmol) was converted to **35** according to procedures H and J. After column chromatography purification using a gradient of 10%→30% Acetone/Hex a yellowish oil was recovered (R_f=0.25 at 10% Acetone/Hex, 100 mg, 0.315 mmol). Yield: 50%; ^{1}H NMR (250 MHz, $CDCl_3$) *δ* 10.24 (s, 1H), 4.68 – 4.54 (m, 1H), 4.52 (d, *J* = 2.7 Hz, 1H), 3.76 (s, 3H), 3.14 – 2.77 (m, 1H), 2.77 – 2.56 (m, 1H), 1.54 (s, 3H), 1.52 (s, 3H), 1.44 (s, 9H). ^{13}C NMR (63 MHz, $CDCl_3$) *δ* 176.1, 171.0, 151.4, 96.1, 81.2, 78.0, 56.3, 52.7, 37.6, 28.4

(S)-methyl 2-((S)-2-((2S,3R)-3-amino-2-hydroxy-5-((2-hydroxyethyl)amino)-5-oxopentanamido)-4-methylpentanamido)-3-(1H-indol-3-yl)propanoate (37a): 24 (20 mg, 0,065 mmol) was converted to **37a** according to general procedures H, J, D, C, D and F. After purification with column chromatography using a gradient of 10→20% MeOH/CH_2Cl_2 and was isolated as amorphous yellowish solid (R_f= 0.7 at 30% MeOH / CH_2Cl_2, 6.5 mg, 0.012 mmol). Yield: 18%. ^1H NMR (250 MHz, Methanol-d_4) δ 7.55 – 7.47 (m, 1H), 7.35 – 7.29 (m, 1H), 7.14 – 6.98 (m, 3H), 4.73 (dd, J = 7.8, 5.7 Hz, 1H), 4.45 (t, J = 7.4 Hz, 1H), 4.04 (d, J = 4.4 Hz, 1H), 3.66 (s, 3H), 3.65 – 3.58 (m, 2H), 3.56 – 3.47 (m, 1H), 3.37 – 3.26 (m, 3H), 3.19 (dd, J = 14.6, 7.8 Hz, 1H), 2.52 (dd, J = 15.1, 4.8 Hz, 1H), 2.32 (dd, J = 15.1, 8.4 Hz, 1H), 1.68 – 1.50 (m, 3H), 0.94 (d, J = 6.4 Hz, 3H), 0.91 (d, J = 6.4 Hz, 3H). ^{13}C NMR (63 MHz, MeOD) δ 174.6, 174.2, 173.8, 173.6, 138.0, 128.7, 124.7, 122.4, 119.9, 119.1, 112.3, 110.5, 73.7, 61.4, 54.9, 53.0, 52.8, 52.7, 43.0, 41.9, 38.6, 28.4, 25.9, 23.3, 22.1. ESI HRMS: *m/z* [M + H]+ calcd for $C_{25}H_{38}N_5O_7^+$, 520.2766; found, 520.2767

(S)-methyl 2-((S)-2-((2S,3R)-3-amino-5-((1,3-dihydroxypropan-2-yl)amino)-2-hydroxy-5-oxopentanamido)-4-methylpentanamido)-3-(1H-indol-3-yl)propanoate (37b): 24 (20 mg, 0,065 mmol) was converted to **37b** according to general procedures H, J, D, C, D and F. After purification with column chromatography using a gradient of 5→20% MeOH/CH_2Cl_2 and was isolated as amorphous yellowish solid (R_f= 0.57 at 30% MeOH / CH_2Cl_2, 10 mg, 0.018 mmol). Yield: 29%. ^1H NMR (250 MHz, Methanol-d_4) δ 7.51 (d, J = 7.6 Hz, 1H), 7.33 (d, J = 7.9 Hz, 1H), 7.17 – 6.93 (m, 3H), 4.73 (dd, J = 7.8, 5.7 Hz, 1H), 4.45 (t, J = 7.4 Hz, 1H), 4.04 – 3.89 (m, 2H), 3.66 (s, 3H), 3.68 – 3.55 (m, 4H), 3.50 – 3.38 (m, 1H), 3.37 – 3.27 (m, 1H), 3.18 (dd, J = 14.6, 7.8 Hz, 1H), 2.47 (dd, J = 14.7, 4.8 Hz, 1H), 2.30 (dd, J = 14.7, 8.2 Hz, 1H), 1.69 – 1.52 (m, 3H), 0.98 – 0.86 (m, 9H). ^{13}C NMR (63 MHz, MeOD) δ 174.6, 174.6, 174.0, 173.8, 138.0, 128.7, 124.7, 122.4, 119.9, 119.1, 112.3, 110.5, 74.5, 62.1, 62.1, 54.8, 54.6, 52.9, 52.7, 41.9, 39.7, 28.4, 25.9, 23.3, 22.1. ESI HRMS: *m/z* [M + H]+ calcd for $C_{26}H_{40}N_5O_8^+$, 550.2872; found, 550.2873

(S)-methyl 2-((S)-2-((2S,3R)-3-amino-2-hydroxy-4-((2-hydroxyethyl)amino)butanamido)-4-methylpentanamido)-3-(1H-indol-3-yl)propanoate (41a): 17 (40 mg, 0,14 mmol) was converted to **41a** according to general procedures C, D, H, L and F. After purification with column chromatography using a gradient of 15→40% MeOH/CH_2Cl_2 and was isolated as amorphous white solid (R_f= 0.12 at 20% MeOH / CH_2Cl_2, 11.0 mg, 0.020 mmol). Yield: 14 %. ^1H NMR (500 MHz, MeOD) δ 7.51 (d, J = 7.8 Hz, 1H), 7.33 (d, J = 8.1 Hz, 1H), 7.13 – 7.06 (m, J = 14.2, 6.3 Hz, 2H), 7.01 (dd, J = 7.4 Hz, 1H), 4.72 (dd, J = 7.5, 5.8 Hz, 1H), 4.45 (dd, J = 7.4 Hz, 1H), 4.13 (d, J = 3.3 Hz, 1H), 3.81 – 3.70 (m, 2H), 3.66 (s, J = 17.4 Hz, 3H), 3.44 – 3.38 (m, 1H), 3.35 – 3.27 (m, J = 16.1, 14.7 Hz, 1H), 3.20 (dd, J = 14.7, 7.8 Hz, 1H), 3.13 (dd, J = 12.6, 4.1 Hz, 1H), 3.07 – 2.98 (m, 2H), 2.93 (dd, J = 12.4, 9.9 Hz, 1H), 1.60 (ddd, J = 27.5, 13.9, 6.7 Hz, 3H), 0.94 (d, J = 6.4 Hz, 3H), 0.91 (d, J = 6.4 Hz, 3H). ^{13}C NMR (126 MHz, D_2O) δ 173.2, 172.5, 172.5, 136.7, 127.4, 123.4, 121.2, 118.6, 117.8, 111.1, 109.3, 71.3, 57.5, 53.6, 51.9, 51.5, 51.2, 49.8, 49.0, 40.6, 27.1, 24.6, 22.0, 20.8. ESI HRMS: *m/z* [M + H]+ calcd for $C_{24}H_{38}N_5O_6^+$, 492.2817; found, 492.2841

(S)-methyl 2-((S)-2-((2S,3R)-3-amino-4-((1,3-dihydroxypropan-2-yl)amino)-2-hydroxybutanamido)-4-methylpentanamido)-3-(1H-indol-3-yl)propanoate (41b): 17 (20 mg, 0,07 mmol) was converted to **41b** according to general procedures C, D, H, L and F. After purification with column chromatography using a gradient of 20→40% MeOH/CH_2Cl_2 and was isolated as amorphous white solid (R_f= 0.4 at 30% MeOH / CH_2Cl_2, 10.0 mg, 0.020 mmol). Yield: 28 %. ^{1}H NMR (250 MHz, MeOD) δ 7.52 (d, *J* = 7.5 Hz, 1H), 7.33 (d, *J* = 7.7 Hz, 1H), 7.12 – 6.96 (m, 3H), 4.72 (dd, *J* = 7.8, 5.8 Hz, 1H), 4.45 (dd, *J* = 7.5 Hz, 1H), 4.15 (d, *J* = 4.0 Hz, 1H), 3.72 – 3.62 (m, 2H), 3.66 (s, 3H), 3.62 – 3.52 (m, 2H), 3.42 – 3.26 (m, 2H), 3.19 (dd, *J* = 14.7, 7.9 Hz, 1H), 3.08 (dd, *J* = 13.0, 4.4 Hz, 1H), 2.90 – 2.76 (m, 2H), 1.71 – 1.51 (m, 3H), 0.94 (d, *J* = 6.3 Hz, 3H), 0.91 (d, *J* = 6.3 Hz, 3H). ^{13}C NMR (63 MHz, MeOD) *δ* 174.5, 173.8, 173.6, 138.0, 128.7, 124.7, 122.4, 119.9, 119.1, 112.4, 110.5, 71.8, 62.2, 61.5, 61.2, 54.9, 54.1, 53.1, 52.7, 47.8, 41.9, 28.3, 25.9, 23.3, 22.1. ESI HRMS: *m/z* [M + H]+ calcd for $C_{25}H_{40}N_5O_7^+$, 522.2922; found, 522.2944

(4S,7S,10S,11R)-4-((1H-indol-3-yl)methyl)-11-amino-10-hydroxy-7-isobutyl-3,6,9-trioxo-2-oxa-5,8,14-triazaheptadecan-17-oic acid (41c): 24 (20 mg, 0,065 mmol) was converted to **41c** according to general procedures C, D, H, L, D and F. After purification with column chromatography using a gradient of 5→20% MeOH/CH_2Cl_2 and was isolated as amorphous white-brown solid (R_f= 0.46 at 25% MeOH / CH_2Cl_2, 7.0 mg, 0.013 mmol). Yield: 20 %. ^{1}H NMR (250 MHz, MeOD) δ 7.55 – 7.48 (m, 1H), 7.36 – 7.30 (m, 1H), 7.14 – 6.96 (m, 3H), 4.71 (dd, *J* = 7.7, 5.7 Hz, 1H), 4.45 (dd, *J* = 7.4 Hz, 1H), 4.06 (d, *J* = 3.5 Hz, 1H), 3.76 – 3.68 (m, 1H), 3.66 (s, 3H), 3.31 (p, *J* = 1.7 Hz, 1H), 3.19 (dd, *J* = 14.7, 7.7 Hz, 1H), 3.10 – 2.92 (m, 4H), 2.65 (dd, *J* = 6.5 Hz, 2H), 1.88 – 1.49 (m, 5H), 0.94 (d, *J* = 6.3 Hz, 3H), 0.91 (d, *J* = 6.3 Hz, 3H).^{13}C NMR (63 MHz, MeOD) δ 174.5, 174.3, 173.8, 173.4, 138.0, 128.7, 124.7, 122.5, 119.9, 119.1, 112.3, 110.5, 73.8, 55.2, 54.9, 53.0, 52.7, 52.5, 47.8, 44.5, 41.9, 33.6, 28.3, 25.9, 23.3, 22.0. ESI HRMS: *m/z* [M + H]+ calcd for $C_{26}H_{40}N_5O_7^+$, 534.2922; found, 534.2915

(S)-methyl 2-((S)-2-((2S,3R)-3-amino-5-((1,3-dihydroxypropan-2-yl)amino)-2-hydroxypentanamido)-4-methylpentanamido)-3-(1H-indol-3-yl)propanoate (41d): 24 (20 mg, 0,065 mmol) was converted to **41d** according to general procedures C, D, H, L and F. After purification with column chromatography using a gradient of 5→30% MeOH/CH_2Cl_2 and was isolated as amorphous white-yellowish solid (R_f= 0.33 at 20% MeOH / CH_2Cl_2, 6.0 mg, 0.01 mmol). Yield: 15 %. ^{1}H NMR (250 MHz, MeOD) *δ* 7.51 (d, *J* = 7.7 Hz, 1H), 7.33 (d, *J* = 8.0 Hz, 1H), 7.16 – 6.94 (m, 3H), 4.71 (dd, *J* = 7.6, 5.4 Hz, 1H), 4.46 (dd, *J* = 7.3 Hz, 1H), 4.06-3.54 (m, 9H), 3.27-2.97 (m, 5H), 1.89 – 1.47 (m, 5H), 0.97 – 0.86 (m, 6H). ^{13}C NMR (63 MHz, MeOD) *δ* 174.6, 174.5, 173.8, 138.0, 128.7, 124.6, 122.5, 119.9, 119.1, 112.3, 110.5, 74.4, 61.7, 60.4, 60.2, 55.4, 54.9, 53.0, 52.7, 49.9, 45.6, 41.9, 28.3, 25.9, 23.3, 22.0. ESI HRMS: *m/z* [M + H]+ calcd for $C_{26}H_{42}N_5O_7^+$, 536.3079; found, 536.3074

(S)-methyl 2-((S)-2-((2S,3R)-3-amino-2-hydroxy-5-((2-hydroxyethyl)amino)pentanamido)-4-methylpentanamido)-3-(1H-indol-3-yl)propanoate (41e): 24 (20 mg, 0,065 mmol) was converted to **41e** according to general procedures C, D, H, L, D and F. After purification with column chromatography using a gradient of 20→40% MeOH/CH_2Cl_2/ 5% aq. NH_4OH and was isolated as amorphous white-yellowish solid (R_f= 0.16 at 20% MeOH / CH_2Cl_2, 4.0 mg, 0.008 mmol). Yield: 12 %. ^{1}H NMR (250 MHz, Methanol-*d*$_4$) δ 7.54 – 7.48 (m, 1H), 7.35 – 7.29 (m, 1H), 7.13 – 6.97 (m, 3H), 4.72 (dd, *J* = 7.6, 5.7 Hz, 1H), 4.45 (dd, *J* = 7.4 Hz, 1H), 3.95 (d, *J* = 3.0 Hz, 1H), 3.68 – 3.63 (m, 2H), 3.65 (s, 3H), 3.36 – 3.25 (m, 1H), 3.19 (dd, *J* = 14.7, 7.7 Hz, 1H), 3.11 – 3.02 (m, 1H), 2.82 – 2.63 (m, 4H), 1.83 – 1.49 (m, 5H), 0.97 – 0.86 (m, 6H). ^{13}C NMR (63 MHz, MeOD) δ 175.3, 174.5, 173.8, 138.0, 128.7, 124.6, 122.4, 119.9, 119.1, 112.3, 110.5, 75.0, 61.3, 54.8, 53.7, 52.8, 52.7, 52.1, 47.1, 42.0, 34.0, 28.3, 25.9, 23.3, 22.1. ESI HRMS: *m/z* [M + H]+ calcd for $C_{25}H_{40}N_5O_6^+$, 506.2973; found, 506.2998

(S)-methyl 2-((S)-2-((2S,3R)-3-amino-2-hydroxy-5-((2-hydroxyethyl)(methyl)amino)pentanamido)-4-methylpentanamido)-3-(1H-indol-3-yl)propanoate (41f): 24 (20 mg, 0,065 mmol) was converted to **41f** according to general procedures C, D, H, L, D and F. After purification with column chromatography using a gradient of 10→20% MeOH/CH_2Cl_2 and was isolated as amorphous white solid (R_f= 0.28 at 20% MeOH / CH_2Cl_2, 5.0 mg, 0.009 mmol). Yield: 14%. ^{1}H NMR (250 MHz, MeOD) δ 7.58 – 7.46 (m, 1H), 7.33 (d, *J* = 7.8 Hz, 1H), 7.15 – 6.95 (m, 3H), 4.72 (dt, *J* = 7.9, 5.3 Hz, 1H), 4.46 (dd, *J* = 7.4 Hz, 1H), 4.11 (d, *J* = 4.4 Hz, 1H), 3.89 – 3.79 (m, 1H), 3.76 – 3.69 (m, 2H), 3.67 (s, 3H), 3.48 – 3.12 (m, 3H), 3.04 – 2.62 (m, 4H), 2.47 (s, 2H) 1.85 – 1.45 (m, 5H), 0.98 – 0.88 (m, 6H). ^{13}C NMR (63 MHz, MeOD) δ 174.5, 173.7, 173.5, 138.0, 128.7, 124.7, 122.5, 119.9, 119.1, 112.4, 110.6, 72.7, 59.4, 58.2, 56.5, 55.8, 54.9, 53.1, 52.7, 41.9, 41.1, 28.3, 26.2, 25.9, 23.3, 22.1. ESI HRMS: *m/z* [M + H]+ calcd for $C_{26}H_{42}N_5O_6^+$, 520.3130; found, 520.3128

(S)-methyl 2-(((2R,3S)-4-(((S)-1-(((S)-3-(1H-indol-3-yl)-1-methoxy-1-oxopropan-2-yl)amino)-4-methyl-1-oxopentan-2-yl)amino)-2-amino-3-hydroxy-4-oxobutyl)amino)-3-(4-hydroxyphenyl)propanoate (41g): 17 (20 mg, 0,07 mmol) was converted to **41g** according to general procedures C, D, H, L and F. After purification with column chromatography using a gradient of 10→30% MeOH/CH_2Cl_2 and was isolated as amorphous white solid (R_f= 0.17 at 10% MeOH / CH_2Cl_2, 9.0 mg, 0.014 mmol). Yield: 22%. ^{1}H NMR (250 MHz, MeOD) δ 7.52 (d, *J* = 7.5 Hz, 1H), 7.33 (d, *J* = 7.7 Hz, 1H), 7.14 – 6.95 (m, 5H), 6.76 – 6.67 (m, *J* = 6.6, 4.7 Hz, 2H), 4.71 (dd, *J* = 7.6, 5.9 Hz, 1H), 4.43 (t, *J* = 7.4 Hz, 1H), 4.13 (d, *J* = 4.4 Hz, 1H), 3.65 (s, 6H), 3.49 (tl, *J* = 6.7 Hz, 1H), 3.4 – 3.14 (m, 3H), 2.98 – 2.82 (m, 3H), 2.58 (dd, *J* = 13.1, 9.4 Hz, 1H), 1.68 – 1.48 (m, 3H), 0.92 (d, *J* = 6 Hz, 6H) ^{13}C NMR (63 MHz, MeOD) δ 176.3, 174.3, 173.8, 172.8, 157.4, 138.0, 131.3, 129.0, 128.7, 124.6, 122.4, 119.9, 119.1, 116.3, 112.3, 110.5, 70.0, 64.6, 55.0, 53.0, 52.7, 52.3, 47.7, 41.9, 39.4, 30.8, 28.3, 25.8, 23.2, 22.2. ESI HRMS: *m/z* [M + H]+ calcd for $C_{32}H_{44}N_5O_8^+$, 626.3185; found, 626.3207

(S)-methyl 2-(((3R,4S)-5-(((S)-1-(((S)-3-(1H-indol-3-yl)-1-methoxy-1-oxopropan-2-yl)amino)-4-methyl-1-oxopentan-2-yl)amino)-3-amino-4-hydroxy-5-oxopentyl)amino)-3-(4-hydroxyphenyl)propanoate (41h): 24 (20 mg, 0,065 mmol) was converted to **41h** according to general procedures C, D, H, L, D and F. After purification with column chromatography using a gradient of 5→10% MeOH/CH_2Cl_2 and was isolated as amorphous white-yellowish solid (R_f= 0.28 at 10% MeOH / CH_2Cl_2, 23.0 mg, 0.036 mmol). Yield: 55%. ^{1}H NMR (250 MHz, MeOD) δ 7.57 – 7.45 (m, 1H), 7.37 – 7.27 (m, 1H), 7.13 – 6.97 (m, 5H), 6.79 – 6.71 (m, 2H), 4.70 (dd, *J* = 7.8, 5.8 Hz, 1H), 4.41 (dd, *J* = 8.2, 6.7 Hz, 1H), 4.24 (d, *J* = 4.8 Hz, 1H), 4.13 (dd, *J* = 7.5, 5.6 Hz, 1H), 3.71 (s, 3H), 3.65 (s, 3H), 3.59 – 3.50 (m, 1H), 3.38 – 3.24 (m, 2H), 3.24 – 2.97 (m, 4H), 2.26 – 1.91 (m, 2H), 1.75 – 1.50 (m, 3H), 0.95 (d, *J* =6.2 Hz, 3H), 0.92 (d, *J* =6.2 Hz, 3H). ^{13}C NMR (63 MHz, MeOD) δ 174.6, 173.8, 172.9, 170.6, 158.3, 138.0, 131.5, 128.6, 125.5, 124.7, 122.5, 119.9, 119.1, 116.8, 112.4, 110.5, 70.7, 62.8, 55.0, 53.5, 53.5, 53.1, 52.8, 44.7, 41.7, 36.4, 28.3, 27.3, 25.9, 23.2, 22.0. ESI HRMS: *m/z* [M + H]+ calcd for $C_{33}H_{46}N_5O_8^+$, 640.3341; found, 640.3349

(S)-2-(((3R,4S)-3-amino-5-(((S)-1-(((S)-1-carboxy-2-(1H-indol-3-yl)ethyl)amino)-4-methyl-1-oxopentan-2-yl)amino)-4-hydroxy-5-oxopentyl)amino)-3-(4-hydroxyphenyl)propanoic acid (41i): 24 (20 mg, 0,065 mmol) was converted to **41i** according to general procedures C, D, H, L, D and F. After purification with column chromatography using a gradient of 20→40% MeOH/CH_2Cl_2/2% aq. NH_4OH and was isolated as amorphous white-yellowish solid (R_f= 0.05 at 20% MeOH / CH_2Cl_2, 23.0 mg, 0.036 mmol). Yield: 55%. ^{1}H NMR (250 MHz, Acetic Acid-*d*$_4$) δ 7.57 (d, *J* = 7.5 Hz, 1H), 7.35 (d, *J* = 8.0 Hz, 1H), 7.20 – 6.96 (m, 5H), 6.78 (d, *J* = 8.1 Hz, 2H), 4.91 (dd, *J* = 7.2, 5.1 Hz, 1H), 4.59 – 4.47 (m, 2H), 4.17 (dd, *J* = 5.9 Hz, 1H), 3.92 – 3.76 (m, 1H), 3.48 – 3.10 (m, 6H), 2.30 – 2.12 (m, 2H), 1.69 – 1.53 (m, 3H), 0.89 (d, *J* = 5.6 Hz, 3H), 0.84 (d, *J* = 5.6 Hz, 3H). ^{13}C NMR (63 MHz, Acetic) δ 176.8, 174.2, 173.8, 173.2, 157.1, 137.4, 131.9, 128.5, 126.2, 124.7, 122.6, 120.1, 119.3, 116.7, 112.3, 110.1, 69.9, 64.8, 54.4, 53.4, 52.6, 44.9, 41.1, 36.2, 28.0, 26.7, 25.5, 23.1, 22.0. ESI HRMS: *m/z* [M + H]+ calcd for $C_{31}H_{42}N_5O_8^+$, 612.3028; found, 612.3031

Protein Expression and Purification

ERAP1 and ERAP2 were expressed and purified from insect cell culture (Hi5 cells) after infection by recombinant baculovirus as previously described.[68] The extracellular enzymatic domain of IRAP was expressed by stably-transfected HEK 293S GnTI$^{(-)}$ cells and purified by affinity chromatography as previously described.[69] All enzymes were stored at –80 °C in 10 mM Hepes (pH 7.5) and 150 mM NaCl, 10% glycerol until needed. For structure determination, an optimized construct for ERAP1 was used in which the exon 10 loop had been substituted by the linker GSG as previously described.[61]

Enzymatic assays

For the determination of the inhibitory potency of the compounds, the enzymatic activity of ERAP1, ERAP2 and IRAP was calculated by following the change in fluorescent signal produced upon digestion of the substrates L-leucine 7-amido-4-methyl coumarin or L-arginine-7-amido-4-methylcoumarin (L-AMC or R-AMC, Sigma-Aldrich). Measurements were performed on a TECAN spark 10M microplate fluorescence reader, following emission at 460 nm, with the excitation set at 380 nm, as previously described.[68,69] To calculate the inhibitory efficacy of each compound, the activity of the enzyme was measured in the presence of increasing concentrations of the inhibitor and data were fit to a 4-parameter variable slope inhibition model using Graphpad Prism™. As a positive control for the *in vitro* assay we used DG013A, a potent but non-selective transition-state analogue inhibitor (**2**, Figure S1).[31]

Cross-presentation assay

HEK293 cells stably transfected to express H-2Kb and murine Fc gamma RII [66] were a kind of gift of Prof. Peter Cresswell, Yale University. IRAP-deficient HEK cells were produced using CRISPR-Cas9 technology and confirmed by sequencing (Jacqueline Leib and Peter van Endert, *manuscript in preparation*). Immune complexes of ovalbumin (Worthington) and rabbit IgG anti-ovalbumin (Polysciences) were formed by incubation on ice for 4 h at a weight ratio of 10:1. WT and IRAP-deficient HEK cells were pulsed for 1 h in DMEM with 1% FCS with immune complexes at an IgG concentration of 250 μg/mL and graded concentrations of inhibitors, washed in PBS and incubated overnight in DMEM with 10% FCS in the presence of inhibitors. Finally, B3Z hybridoma cells were added at a ratio of 1:1 and incubated for 24 h with immune complex-pulsed HEK cells. IL-2 production by B3Z cells was determined by sandwich ELISA.

Protein expression, crystallization and X-ray diffraction experiments

ERAP1 was produced by insect cell culture and purified as previously reported.[61] ERAP1 was co-crystallized in complex with compound **30** by the sitting-drop vapor-diffusion method in 100 mM DL-malic acid, Bis-tris propane, pH 7.0, 25% PEG 1500 at a protein concentration of 12 mg/mL and a molar ratio of protein to ligand of 1:5, as previously described.[61] Crystals were cryoprotected using a solution of the precipitant and 20% ethylene glycol and subsequently flash frozen in liquid N_2. Data were collected at 100 K at a wavelength of 1.0 Å on beamline P13 of PETRA III at EMBL, Hamburg, Germany. Data processing, structure determination and refinement were performed as previously described.[61]

IRAP was isolated after secretion from stably-transfected HEK 293S GnTI(-) cells and purified by affinity and size-exclusion chromatography as previously reported.[58] Crystals of IRAP complexes with compound **32e** were achieved after screening procedure against the commercially available PACT-premier crystallization screen (Molecular Dimensions™). Crystals were grown at 16 °C by the sitting-drop vapor-diffusion method in 0.1 M MMT buffer (Malic acid, Tris, MES), pH 5.0 and 25% (w/v) polyethylene glycol (PEG) of mean MW 1500 Da (D2 condition). One hour prior to crystallization trials, purified IRAP concentrated at 9.8 mg/mL was mixed with the inhibitor at a molar ratio 1:5 and the mixture was kept at 4 °C. Cryoprotection was achieved by rapid immersion in a solution containing the precipitant and 20% ethylene glycol for a period of 5–10 s, and subsequently the crystals were flash frozen in liquid N_2. Frozen crystals were shipped in a Taylor-Wharton CX100 dry shipper to the Synchrotron facility. Datasets were collected at 100 K at a wavelength of 0.976 Å on beamline P13 of Petra III, EMBL, Hamburg, Germany. The reflections were integrated with XDS, the space group was determined with POINTLESS and the data merging was accomplished with STARANISO (http://staraniso.globalphasing.org). The best resulting dataset displayed data to 2.3 Å. The crystals belonged to space group P 1 21 1 with a=73.478 Å, b=120.051, c=141.246 Å, and β=103.281°. The structure was solved by molecular replacement with PHASER using as a search model the closed structure of IRAP (PDB ID: 5MJ6). Two protein molecules were found in the asymmetric unit (referred to as chains A and B). Inspection of the initial electron density maps showed the presence of strong additional electron density adjacent to the catalytic Zn(II) atom, which was attributed to the inhibitor. Two different conformations the inhibitor were built in chain B (discussed in main text). Structure refinement was conducted with PHENIX using restrained refinement and non-crystallographic symmetry restraints, while at the final stages TLS refinement was included. Model building and real-space refinement were performed in Coot. Due to low data completeness at 2.3 Å, the high-resolution limit was set to 2.8 Å. In chain A no density was visible before residue 158 and for residues 223–226, 598–599 and 639–648, while in chain B no density was visible prior to residue 158 and for residues 223–226, 340 and 638–648. The final model includes 29 molecules of *N*-acetyl-D-glucosamine, 5 of β-D-mannose, 5 of α-D-mannopyranose, one 2-amino-2-hydroxymethyl-propane-1,3-diol (Tris), three polyethylene glycol, 7 molecules of 1,2-ethanediol and 105 water molecules.

ASSOCIATED CONTENT

Supporting Information. Titration curves of key compounds and potent inhibitors with the 3 enzymes (Figure S1); Data collection and refinement statistics of the two X-ray crystal structures (Tables S1, S2); Illustration of ERAP1 active site in complex with **30** (Figure S2); Electron density in the active site of IRAP in complex with **32e** (Figure S3); HPLC retention times and the ESI–HRMS *m/z* detected for the final compounds (Table S3); HPLC traces of key compounds and potent inhibitors; ^{1}H and ^{13}C NMR spectra of all final compounds. Molecular Formula Strings of the final compounds are provided as CSV file.

Accession Codes. Coordinates and structure factors of ERAP1 in complex with **30**, and IRAP in complex with **32e** have been deposited in the Protein Data Bank under accession numbers 7Z28 and 7ZYF, respectively. Authors will release the atomic coordinates upon article publication.

AUTHOR INFORMATION

Corresponding Authors

* Efstratios Stratikos, Department of Chemistry, National and Kapodistrian University of Athens, Panepistimioupolis Zografou, GR-15784 Athens, Greece, ORCID: 0000-0002-3566-2309, Email: estratikos@chem.uoa.gr

* Athanasios Papakyriakou, Institute of Biosciences & Applications, National Centre for Scientific Research "Demokritos", Agia Paraskevi Attikis, GR-15341 Athens, Greece, ORCID: 0000-0003-3931-6232, Email: thpap@bio.demokritos.gr

Author Contributions

DV[‡], IM[‡] and AA performed the synthesis and characterization of the compounds; DK and IT performed the biochemical assays and processed data; PG and AM carried out the crystallization of the complexes and solved the X-ray structures; VM performed ESI HRMS measurements and characterization of the compounds; JL and PvE performed the cross-presentation assay; DV, ES and AP conceptualized the project, processed and interpreted data, and wrote the manuscript with contribution from all authors. All authors have given approval to the final version of the manuscript. [‡]The first two authors contributed equally.

Funding sources

AA, AM and AP have been funded by the Hellenic Foundation for Research and Innovation (HFRI) under the 1st call Support for Postdoctoral Researchers, grant "ARIA" number 303. The authors also acknowledge financial support by the project "NCSRD—INRASTES research activities in the framework of the national RIS3” (MIS 5002559) which is implemented under the “Action for the Strategic Development on the Research and Technological Sector”, funded by the Operational Programme “Competitiveness, Entrepreneurship and Innovation” (NSRF 2014-2020) and co-financed by Greece and the European Union (European Regional Development Fund). We also acknowledge support of this work by the project “INSPIRED-The National Research Infrastructures on Integrated Structural Biology, Drug Screening Efforts and Drug Target Functional Characterization” (Grant MIS 5002550), which is implemented under the Action “Reinforcement of the Research and Innovation Infrastructure”, funded by the Operational Programme “Competitiveness, Entrepreneurship and Innovation” (Grant NSRF 2014−2020) and co-financed by Greece and the European Union (European Regional Development Fund). PvE. was supported by grant ANR-20-CE18-0003-03 from the Agence Nationale de Recherche and grant DCM2018039548 from the Fondation pour la Recherche Médicale. Access to the EMBL Hamburg beamline P13 has been supported by iNEXT-Discovery PID 5589, project number 871037, funded by the Horizon 2020 program of the European Commission.

Notes

The authors declare no competing financial interest.

ACKNOWLEDGMENT

We would like to thank GlaxoSmithKline and in particular Drs Semra Kitchen and Jonathan P. Hutchinson for their generous gift of ERAP1 enzyme used in crystallization experiments. EMBL Hamburg is kindly acknowledged for providing access to beamline P13 under the BAG proposal MX-726. Dr. Emmanuel Pitsinos is kindly acknowledged for his critical comments on the manuscript.

ABBREVIATIONS USED

APA, aminopeptidase A; APN, aminopeptidase N; CAN, ceric ammonium nitrate; DCDMH, 1,3-Dichloro-5,5-dimethyl-2,4-imidazolidinedione; $(DHQD)_2PHAL$, hydroquinidine 1,4-phthalazinediyl diether; DIAD, diisopropyl azodicarboxylate; DIPEA, *N*,*N*-diisopropylethylamine; DMF, dimethylformamide; DCM, dichloromethane; DMSO, dimethyl sulfoxide; ERAP1/2; endoplasmic reticulum aminopeptidase 1/2; EtOAc, ethyl acetate; EtOH, ethanol; ESI, electrospray ionization; HATU, 1-[Bis(dimethylamino)methylene]-1*H*-1,2,3-triazolo[4,5-*b*]pyridinium 3-oxid hexafluorophosphate; HPLC, high-performance liquid chromatography; HRMS, high-resolution mass spectrometry; IRAP, insulin regulated aminopeptidase; K/LiHDMS: Potassium/Lithium 1,1,1-trimethyl-*N*-(trimethylsilyl)silanaminide; NBS, *N*-Bromosuccinimide; NMR, nuclear magnetic resonance; PPTS, pyridinium *p*-toluenesulfonate; rt, room temperature; TEA, trimethylamine; TFA, trifluoroacetic acid; THF, tetrahydrofuran; TLC, thin layer chromatography.

REFERENCES

1. *Aminopeptidases in Biology and Disease*; 1 ed.; Springer, Boston, MA, 2004. ISBN 978-0-306-48465-0, doi: 10.1007/978-1-4419-8869-0

2. Drinkwater N, Lee J, Yang W, Malcolm TR, McGowan S. M1 Aminopeptidases as Drug Targets: Broad Applications or Therapeutic Niche? *FEBS J* (2017) **284:**1473-1488. doi:10.1111/febs.14009

3. Laura M, Ronan G, Vy LB, Valentin G, Omar CA, Virgyl C, Piveteau C, Melissa R, Charlotte F, Sandrine W, Julie C, Julie DR, Damien B, Florence L, Peter VE, Benoit D, Rebecca DP. Modulators of Herap2 Discovered by High-Throughput Screening. *Eur J Med Chem* (2021) **211:**113053. doi:10.1016/j.ejmech.2020.113053

4. Maben Z, Arya R, Rane D, An WF, Metkar S, Hickey M, Bender S, Ali A, Nguyen TT, Evnouchidou I, Schilling R, Stratikos E, Golden J, Stern LJ. Discovery of Selective Inhibitors of Endoplasmic Reticulum Aminopeptidase 1. *J Med Chem* (2020) **63:**103-121. doi:10.1021/acs.jmedchem.9b00293

5. Zervoudi E, Saridakis E, Birtley JR, Seregin SS, Reeves E, Kokkala P, Aldhamen YA, Amalfitano A, Mavridis IM, James E, Georgiadis D, Stratikos E. Rationally Designed Inhibitor Targeting Antigen-Trimming Aminopeptidases Enhances Antigen Presentation and Cytotoxic T-Cell Responses. *Proc Natl Acad Sci U S A* (2013) **110:**19890-19895. doi:10.1073/pnas.1309781110

6. Papakyriakou A, Zervoudi E, Tsoukalidou S, Mauvais FX, Sfyroera G, Mastellos DC, van Endert P, Theodorakis EA, Vourloumis D, Stratikos E. 3,4-Diaminobenzoic Acid Derivatives as Inhibitors of the Oxytocinase Subfamily of M1 Aminopeptidases with Immune-Regulating Properties. *J Med Chem* (2015) **58:**1524-1543. doi:10.1021/jm501867s

7. Chai SY, Yeatman HR, Parker MW, Ascher DB, Thompson PE, Mulvey HT, Albiston AL. Development of Cognitive Enhancers Based on Inhibition of Insulin-Regulated Aminopeptidase. *BMC Neurosci* (2008) **9 Suppl 2:**S14. doi:10.1186/1471-2202-9-S2-S14

8. Andersson H, Hallberg M. Discovery of Inhibitors of Insulin-Regulated Aminopeptidase as Cognitive Enhancers. *Int J Hypertens* (2012) **2012:**789671. doi:10.1155/2012/789671

9. Hanson AL, Morton CJ, Parker MW, Bessette D, Kenna TJ. The Genetics, Structure and Function of the M1 Aminopeptidase Oxytocinase Subfamily and Their Therapeutic Potential in Immune-Mediated Disease. *Hum Immunol* (2019) **80:**281-289. doi:10.1016/j.humimm.2018.11.002

10. Reeves E, Islam Y, James E. Erap1: A Potential Therapeutic Target for a Myriad of Diseases. *Expert Opin Ther Targets* (2020) **24:**535-544. doi:10.1080/14728222.2020.1751821

11. Georgiadis D, Ziotopoulou A, Kaloumenou E, Lelis A, Papasava A. The Discovery of Insulin-Regulated Aminopeptidase (Irap) Inhibitors: A Literature Review. *Front Pharmacol* (2020) **11:**585838. doi:10.3389/fphar.2020.585838

12. Bufalieri F, Infante P, Bernardi F, Caimano M, Romania P, Moretti M, Lospinoso Severini L, Talbot J, Melaiu O, Tanori M, Di Magno L, Bellavia D, Capalbo C, Puget S, De Smaele E, Canettieri G, Guardavaccaro D, Busino L, Peschiaroli A, Pazzaglia S, Giannini G, Melino G, Locatelli F, Gulino A, Ayrault O, Fruci D, Di Marcotullio L. Erap1 Promotes Hedgehog-Dependent Tumorigenesis by Controlling Usp47-Mediated Degradation of Betatrcp. *Nat Commun* (2019) **10:**3304. doi:10.1038/s41467-019-11093-0

13. Chen L, Ridley A, Hammitzsch A, Al-Mossawi MH, Bunting H, Georgiadis D, Chan A, Kollnberger S, Bowness P. Silencing or Inhibition of Endoplasmic Reticulum Aminopeptidase 1 (Erap1) Suppresses Free Heavy Chain Expression and Th17 Responses in Ankylosing Spondylitis. *Ann Rheum Dis* (2016) **75:**916-923. doi:10.1136/annrheumdis-2014-206996

14. Aldhamen YA, Pepelyayeva Y, Rastall DP, Seregin SS, Zervoudi E, Koumantou D, Aylsworth CF, Quiroga D, Godbehere S, Georgiadis D, Stratikos E, Amalfitano A. Autoimmune Disease-Associated Variants of Extracellular Endoplasmic Reticulum Aminopeptidase 1 Induce Altered Innate Immune Responses by Human Immune Cells. *J Innate Immun* (2015) **7:**275-289. doi:10.1159/000368899

15. Saveanu L, Carroll O, Weimershaus M, Guermonprez P, Firat E, Lindo V, Greer F, Davoust J, Kratzer R, Keller SR, Niedermann G, van Endert P. Irap Identifies an Endosomal Compartment Required for Mhc Class I Cross-Presentation. *Science* (2009) **325:**213-217. doi:10.1126/science.1172845

16. Evnouchidou I, Chappert P, Benadda S, Zucchetti A, Weimershaus M, Bens M, Caillens V, Koumantou D, Lotersztajn S, van Endert P, Davoust J, Guermonprez P, Hivroz C, Gross DA, Saveanu L. Irap-Dependent Endosomal T Cell Receptor Signalling Is Essential for T Cell Responses. *Nat Commun* (2020) **11:**2779. doi:10.1038/s41467-020-16471-7

17. Mpakali A, Stratikos E. The Role of Antigen Processing and Presentation in Cancer and the Efficacy of Immune Checkpoint Inhibitor Immunotherapy. *Cancers (Basel)* (2021) **13:**doi:10.3390/cancers13010134

18. Segura E, Albiston AL, Wicks IP, Chai SY, Villadangos JA. Different Cross-Presentation Pathways in Steady-State and Inflammatory Dendritic Cells. *Proc Natl Acad Sci U S A* (2009) **106:**20377-20381. doi:10.1073/pnas.0910295106

19. Lucarini V, Melaiu O, Tempora P, D'Amico S, Locatelli F, Fruci D. Dendritic Cells: Behind the Scenes of T-Cell Infiltration into the Tumor Microenvironment. *Cancers (Basel)* (2021) **13:**doi:10.3390/cancers13030433

20. Hallberg M, Larhed M. From Angiotensin Iv to Small Peptidemimetics Inhibiting Insulin-Regulated Aminopeptidase. *Front Pharmacol* (2020) **11:**590855. doi:10.3389/fphar.2020.590855

21. Barlow N, Thompson PE. Irap Inhibitors: M1-Aminopeptidase Family Inspiration. *Front Pharmacol* (2020) **11:**585930. doi:10.3389/fphar.2020.585930

22. Albiston AL, McDowall SG, Matsacos D, Sim P, Clune E, Mustafa T, Lee J, Mendelsohn FA, Simpson RJ, Connolly LM, Chai SY. Evidence That the Angiotensin Iv (at(4)) Receptor Is the Enzyme Insulin-Regulated Aminopeptidase. *J Biol Chem* (2001) **276:**48623-48626. doi:10.1074/jbc.C100512200

23. Andersson H, Demaegdt H, Vauquelin G, Lindeberg G, Karlen A, Hallberg M, Erdelyi M, Hallberg A. Disulfide Cyclized Tripeptide Analogues of Angiotensin Iv as Potent and Selective Inhibitors of Insulin-Regulated Aminopeptidase (Irap). *J Med Chem* (2010) **53:**8059-8071. doi:10.1021/jm100793t

24. Barlow N, Vanga SR, Savmarker J, Sandstrom A, Burns P, Hallberg A, Aqvist J, Gutierrez-de-Teran H, Hallberg M, Larhed M, Chai SY, Thompson PE. Macrocyclic Peptidomimetics as Inhibitors of Insulin-Regulated Aminopeptidase (Irap). *RSC Med Chem* (2020) **11:**234-244. doi:10.1039/c9md00485h

25. Mountford SJ, Albiston AL, Charman WN, Ng L, Holien JK, Parker MW, Nicolazzo JA, Thompson PE, Chai SY. Synthesis, Structure-Activity Relationships and Brain Uptake of a Novel Series of Benzopyran Inhibitors of Insulin-Regulated Aminopeptidase. *J Med Chem* (2014) **57:**1368-1377. doi:10.1021/jm401540f

26. Albiston AL, Morton CJ, Ng HL, Pham V, Yeatman HR, Ye S, Fernando RN, De Bundel D, Ascher DB, Mendelsohn FA, Parker MW, Chai SY. Identification and Characterization of a New Cognitive Enhancer Based on Inhibition of Insulin-Regulated Aminopeptidase. *FASEB J* (2008) **22:**4209-4217. doi:10.1096/fj.08-112227

27. Diwakarla S, Nylander E, Gronbladh A, Vanga SR, Khan YS, Gutierrez-de-Teran H, Savmarker J, Ng L, Pham V, Lundback T, Jenmalm-Jensen A, Svensson R, Artursson P, Zelleroth S, Engen K, Rosenstrom U, Larhed M, Aqvist J, Chai SY, Hallberg M. Aryl Sulfonamide Inhibitors of Insulin-Regulated Aminopeptidase Enhance Spine Density in Primary Hippocampal Neuron Cultures. *ACS Chem Neurosci* (2016) **7:**1383-1392. doi:10.1021/acschemneuro.6b00146

28. Engen K, Rosenstrom U, Axelsson H, Konda V, Dahllund L, Otrocka M, Sigmundsson K, Nikolaou A, Vauquelin G, Hallberg M, Jenmalm Jensen A, Lundback T, Larhed M. Identification of Drug-Like Inhibitors of Insulin-Regulated Aminopeptidase through Small-Molecule Screening. *Assay Drug Dev Technol* (2016) **14:**180-193. doi:10.1089/adt.2016.708

29. Borhade SR, Rosenstrom U, Savmarker J, Lundback T, Jenmalm-Jensen A, Sigmundsson K, Axelsson H, Svensson F, Konda V, Skold C, Larhed M, Hallberg M. Inhibition of Insulin-Regulated Aminopeptidase (Irap) by Arylsulfonamides. *ChemistryOpen* (2014) **3:**256-263. doi:10.1002/open.201402027

30. Engen K, Vanga SR, Lundback T, Agalo F, Konda V, Jensen AJ, Aqvist J, Gutierrez-de-Teran H, Hallberg M, Larhed M, Rosenstrom U. Synthesis, Evaluation and Proposed Binding Pose of Substituted Spiro-

Oxindole Dihydroquinazolinones as Irap Inhibitors. *ChemistryOpen* (2020) **9:**325-337. doi:10.1002/open.201900344

31. Kokkala P, Mpakali A, Mauvais FX, Papakyriakou A, Daskalaki I, Petropoulou I, Kavvalou S, Papathanasopoulou M, Agrotis S, Fonsou TM, van Endert P, Stratikos E, Georgiadis D. Optimization and Structure-Activity Relationships of Phosphinic Pseudotripeptide Inhibitors of Aminopeptidases That Generate Antigenic Peptides. *J Med Chem* (2016) **59:**9107-9123. doi:10.1021/acs.jmedchem.6b01031

32. Weglarz-Tomczak E, Vassiliou S, Mucha A. Discovery of Potent and Selective Inhibitors of Human Aminopeptidases Erap1 and Erap2 by Screening Libraries of Phosphorus-Containing Amino Acid and Dipeptide Analogues. *Bioorg Med Chem Lett* (2016) **26:**4122-4126. doi:10.1016/j.bmcl.2016.06.062

33. Umezawa H, Aoyagi T, Suda H, Hamada M, Takeuchi T. Bestatin, an Inhibitor of Aminopeptidase B, Produced by Actinomycetes. *J Antibiot (Tokyo)* (1976) **29:**97-99. doi:10.7164/antibiotics.29.97

34. Nishizawa R, Saino T, Takita T, Suda H, Aoyagi T. Synthesis and Structure-Activity Relationships of Bestatin Analogues, Inhibitors of Aminopeptidase B. *J Med Chem* (1977) **20:**510-515. doi:10.1021/jm00214a010

35. Burley SK, David PR, Lipscomb WN. Leucine Aminopeptidase: Bestatin Inhibition and a Model for Enzyme-Catalyzed Peptide Hydrolysis. *Proc Natl Acad Sci U S A* (1991) **88:**6916-6920. doi:10.1073/pnas.88.16.6916

36. Tsuge H, Ago H, Aoki M, Furuno M, Noma M, Miyano M, Minami M, Izumi T, Shimizu T. Crystallization and Preliminary X-Ray Crystallographic Studies of Recombinant Human Leukotriene A4 Hydrolase Complexed with Bestatin. *J Mol Biol* (1994) **238:**854-856. doi:10.1006/jmbi.1994.1341

37. Addlagatta A, Gay L, Matthews BW. Structure of Aminopeptidase N from Escherichia Coli Suggests a Compartmentalized, Gated Active Site. *Proc Natl Acad Sci U S A* (2006) **103:**13339-13344. doi:10.1073/pnas.0606167103

38. Wilkes SH, Prescott JM. The Slow, Tight Binding of Bestatin and Amastatin to Aminopeptidases. *J Biol Chem* (1985) **260:**13154-13162.

39. Ota K. Review of Ubenimex (Bestatin): Clinical Research. *Biomed Pharmacother* (1991) **45:**55-60. doi:10.1016/0753-3322(91)90123-b

40. Sekine K, Fujii H, Abe F. Induction of Apoptosis by Bestatin (Ubenimex) in Human Leukemic Cell Lines. *Leukemia* (1999) **13:**729-734. doi:10.1038/sj.leu.2401388

41. Amin SA, Adhikari N, Jha T. Design of Aminopeptidase N Inhibitors as Anti-Cancer Agents. *J Med Chem* (2018) **61:**6468-6490. doi:10.1021/acs.jmedchem.7b00782

42. Velmourougane G, Harbut MB, Dalal S, McGowan S, Oellig CA, Meinhardt N, Whisstock JC, Klemba M, Greenbaum DC. Synthesis of New (-)-Bestatin-Based Inhibitor Libraries Reveals a Novel Binding Mode in the S1 Pocket of the Essential Malaria M1 Metalloaminopeptidase. *J Med Chem* (2011) **54:**1655-1666. doi:10.1021/jm101227t

43. Lee BW, Lee JH, Jang KC, Kang JE, Kim JH, Park KM, Park KH. Diastereoselective Synthesis of Syn-Aminoalcohols Via Contributing Ch-Pi Interaction: Simple Synthesis of (-)-Bestatin. *Tetrahedron Letters* (2003) **44:**5905-5907. doi:10.1016/S0040-4039(03)01394-7

44. Manickam G, Nogami H, Kanai M, Groger H, Shibasaki M. Anti- and Syn-Selective Cyanosilylation Reactions Promoted by a Sugar-Based Bifunctional Catalyst: Stereoselective Syntheses of Essential Building Blocks for Hiv Protease Inhibitors and Bestatin. *Synlett* (2001) 617-620.

45. Bergmeier SC, Stanchina DM. Acylnitrene Route to Vicinal Amino Alcohols. Application to the Synthesis of (-)-Bestatin and Analogues. *Journal of Organic Chemistry* (1999) **64:**2852-2859. doi:Doi 10.1021/Jo9823893

46. Gogoi N, Boruwa J, Barua NC. A Total Synthesis of (-)-Bestatin Using Shibasaki's Asymmetric Henry Reaction. *Tetrahedron Letters* (2005) **46:**7581-7582. doi:10.1016/j.tetlet.2005.08.153

47. George S, Suryavanshi GS, Sudalai A. A Short Enantioselective Synthesis of (-)-Bestatin Via L-Proline-Catalyzed Alpha-Amination of an Aldehyde. *Tetrahedron Letters* (2008) **49:**6791-6793. doi:10.1016/j.tetlet.2008.09.054

48. Fringuelli F, Pizzo F, Rucci M, Vaccaro L. First One-Pot Copper-Catalyzed Synthesis of Alpha-Hydroxy-Beta-Amino Acids in Water. A New Protocol for Preparation of Optically Active Norstatines. *Journal of Organic Chemistry* (2003) **68:**7041-7045. doi:10.1021/jo034752y

49. Kudyba I, Raczko J, Jurczak J. Asymmetric Nitroaldol Reaction. Synthesis of Taxotere Side Chain and (-)-Bestatin Using (1r)-8-Phenylmenthyl Glyoxylate. *Journal of Organic Chemistry* (2004) **69:**2844-2850. doi:10.1021/jo0358269

50. Wang Q, Huang W, Yuan H, Cai Q, Chen L, Lv H, Zhang X. Rhodium-Catalyzed Enantioselective Hydrogenation of Tetrasubstituted Alpha-Acetoxy Beta-Enamido Esters: A New Approach to Chiral Alpha-Hydroxyl-Beta-Amino Acid Derivatives. *J Am Chem Soc* (2014) **136:**16120-16123. doi:10.1021/ja509005e

51. Semple JE, Owens TD, Nguyen K, Levy OE. New Synthetic Technology for Efficient Construction of Alpha-Hydroxy-Beta-Amino Amides Via the Passerini Reaction. *Org Lett* (2000) **2:**2769-2772. doi:10.1021/ol0061485

52. Feske BD, Stewart JD. Chemoenzymatic Formal Total Synthesis of (-)-Bestatin. *Tetrahedron-Asymmetry* (2005) **16:**3124-3127. doi:10.1016/j.tetasy.2005.08.022

53. Li GG, Chang HT, Sharpless KB. Catalytic Asymmetric Aminohydroxylation (Aa) of Olefins. *Angewandte Chemie-International Edition in English* (1996) **35:**451-454. doi:DOI 10.1002/anie.199604511

54. Shuter EC, Duong H, Hutton CA, McLeod MD. The Enantioselective Synthesis of Apto and Aetd: Polyhydroxylated Beta-Amino Acid Constituents of the Microsclerodermin Cyclic Peptides. *Organic & Biomolecular Chemistry* (2007) **5:**3183-3189. doi:10.1039/b707891a

55. Bodkin JA, Bacskay GB, McLeod MD. The Sharpless Asymmetric Aminohydroxylation Reaction: Optimising Ligand/Substrate Control of Regioselectivity for the Synthesis of 3- and 4-Aminosugars. *Organic & Biomolecular Chemistry* (2008) **6:**2544-2553. doi:10.1039/b803310b

56. Debnar T, Wang T, Menche D. Stereoselective Synthesis of the Butyrolactone and the Oxazoline/Furan Fragment of Leupyrrin a(1). *Org Lett* (2013) **15:**2774-2777. doi:10.1021/ol401110x

57. Zervoudi E, Papakyriakou A, Georgiadou D, Evnouchidou I, Gajda A, Poreba M, Salvesen GS, Drag M, Hattori A, Swevers L, Vourloumis D, Stratikos E. Probing the S1 Specificity Pocket of the Aminopeptidases That Generate Antigenic Peptides. *Biochem J* (2011) **435:**411-420. doi:10.1042/BJ20102049

58. Mpakali A, Saridakis E, Harlos K, Zhao Y, Kokkala P, Georgiadis D, Giastas P, Papakyriakou A, Stratikos E. Ligand-Induced Conformational Change of Insulin-Regulated Aminopeptidase: Insights on Catalytic Mechanism and Active Site Plasticity. *J Med Chem* (2017) **60:**2963-2972. doi:10.1021/acs.jmedchem.6b01890

59. Goto Y, Hattori A, Ishii Y, Mizutani S, Tsujimoto M. Enzymatic Properties of Human Aminopeptidase A. Regulation of Its Enzymatic Activity by Calcium and Angiotensin Iv. *J Biol Chem* (2006) **281:**23503-23513. doi:10.1074/jbc.M603191200

60. Mpakali A, Giastas P, Deprez-Poulain R, Papakyriakou A, Koumantou D, Gealageas R, Tsoukalidou S, Vourloumis D, Mavridis IM, Stratikos E, Saridakis E. Crystal Structures of Erap2 Complexed with Inhibitors Reveal Pharmacophore Requirements for Optimizing Inhibitor Potency. *ACS Med Chem Lett* (2017) **8:**333-337. doi:10.1021/acsmedchemlett.6b00505

61. Giastas P, Neu M, Rowland P, Stratikos E. High-Resolution Crystal Structure of Endoplasmic Reticulum Aminopeptidase 1 with Bound Phosphinic Transition-State Analogue Inhibitor. *ACS Med Chem Lett* (2019) **10:**708-713. doi:10.1021/acsmedchemlett.9b00002

62. Kochan G, Krojer T, Harvey D, Fischer R, Chen L, Vollmar M, von Delft F, Kavanagh KL, Brown MA, Bowness P, Wordsworth P, Kessler BM, Oppermann U. Crystal Structures of the Endoplasmic Reticulum Aminopeptidase-1 (Erap1) Reveal the Molecular Basis for N-Terminal Peptide Trimming. *Proc Natl Acad Sci U S A* (2011) **108:**7745-7750. doi:10.1073/pnas.1101262108

63. Giastas P, Mpakali A, Papakyriakou A, Lelis A, Kokkala P, Neu M, Rowland P, Liddle J, Georgiadis D, Stratikos E. Mechanism for Antigenic Peptide Selection by Endoplasmic Reticulum Aminopeptidase 1. *Proc Natl Acad Sci U S A* (2019) **116:**26709-26716. doi:10.1073/pnas.1912070116

64. Liddle J, Hutchinson JP, Kitchen S, Rowland P, Neu M, Cecconie T, Holmes DS, Jones E, Korczynska J, Koumantou D, Lea JD, Nickels L, Pemberton M, Phillipou A, Schneck JL, Sheehan H, Tinworth CP, Uings I, Wojno-Picon J, Young RJ, Stratikos E. Targeting the Regulatory Site of Er Aminopeptidase 1 Leads to the Discovery of a Natural Product Modulator of Antigen Presentation. *J Med Chem* (2020) **63:**3348-3358. doi:10.1021/acs.jmedchem.9b02123

65. Maben Z, Arya R, Georgiadis D, Stratikos E, Stern LJ. Conformational Dynamics Linked to Domain Closure and Substrate Binding Explain the Erap1 Allosteric Regulation Mechanism. *Nat Commun* (2021) **12:**5302. doi:10.1038/s41467-021-25564-w

66. Giodini A, Rahner C, Cresswell P. Receptor-Mediated Phagocytosis Elicits Cross-Presentation in Nonprofessional Antigen-Presenting Cells. *Proc Natl Acad Sci U S A* (2009) **106:**3324-3329. doi:10.1073/pnas.0813305106

67. Firat E, Saveanu L, Aichele P, Staeheli P, Huai J, Gaedicke S, Nil A, Besin G, Kanzler B, van Endert P, Niedermann G. The Role of Endoplasmic Reticulum-Associated Aminopeptidase 1 in Immunity to Infection and in Cross-Presentation. *J Immunol* (2007) **178:**2241-2248. doi:10.4049/jimmunol.178.4.2241

68. Stamogiannos A, Maben Z, Papakyriakou A, Mpakali A, Kokkala P, Georgiadis D, Stern LJ, Stratikos E. Critical Role of Interdomain Interactions in the Conformational Change and Catalytic Mechanism of Endoplasmic Reticulum Aminopeptidase 1. *Biochemistry* (2017) **56:**1546-1558. doi:10.1021/acs.biochem.6b01170

69. Mpakali A, Saridakis E, Giastas P, Maben Z, Stern LJ, Larhed M, Hallberg M, Stratikos E. Structural Basis of Inhibition of Insulin-Regulated Aminopeptidase by a Macrocyclic Peptidic Inhibitor. *ACS Med Chem Lett* (2020) **11:**1429-1434. doi:10.1021/acsmedchemlett.0c00172

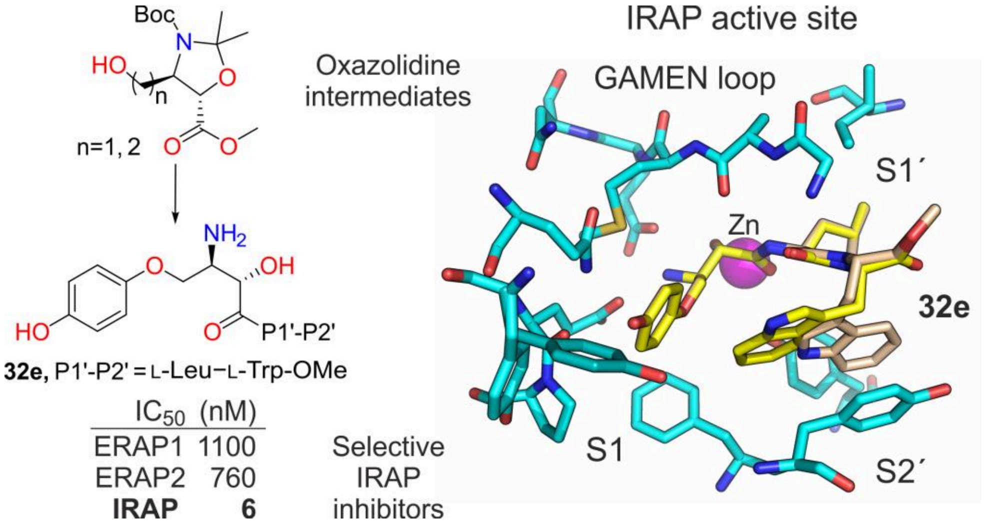Graphic for manuscript